RESEARCH ARTICLE SUMMARY

MICROBIOLOGY

Structural modeling reveals phage proteins that manipulate bacterial immune signaling

Nitzan Tal, Romi Hadary, Renee B. Chang, Ilya Osterman, Roy Jacobson, Erez Yirmiya, Nathalie Bechon, Dina Hochhauser, Miguel López Rivera, Barak Madhala, Jeremy Garb, Moshe Goldsmith, Tanita Wein, Philip J. Kranzusch, Gil Amitai, Rotem Sorek*

Full article and list of author affiliations: https://doi.org/10.1126/science.aea1761

INTRODUCTION: Many innate immune pathways in bacteria, plants, and animals use nucleotide derivatives as intracellular immune signaling molecules. Phages have evolved counterdefense "sponge" proteins that inhibit bacterial immune signaling by binding and sequestering the immune signals as well as enzymes that can cleave and inactivate the signaling molecules. A few antidefense sponge and enzyme protein families were recently discovered serendipitously, suggesting that they are abundant among phages. Our goal was to develop an unbiased approach to computationally predict and experimentally verify previously unknown families of antidefense enzymes and sponge proteins within vast databases of viral protein sequences.

RATIONALE: We reasoned that, despite their divergence in sequence and structure, viral proteins that target nucleotide signals might share common structural and biophysical traits arising from their shared function. By comparing the structures of known viral sponge proteins, we identified unifying features: they are small (typically ≤100 amino acids); form homo-oligomeric assemblies; and have deep, positively charged pockets that bind the negatively charged nucleotide signals. We also found that sponges from different families are frequently encoded fused as a single polypeptide. We hypothesized that these structural fingerprints could be used to discover viral sponges through structural modeling of large sets of viral proteins.

RESULTS: We built a structure-guided computational pipeline that searches viral protein databases either for proteins fused with known sponges or for small, unannotated proteins predicted by AlphaFold-Multimer to form homo-oligomers with internal positively charged pockets. Screening a clustered database of 32 million proteins from 2 million phage genomes resulted in >120 candidate proteins that were experimentally tested for their ability to inhibit bacterial immune signaling. This resulted in the discovery of three previously unidentified families of phage-encoded antidefense proteins. Two families, Sequestin and Lockin, are sponges that sequester the Thoeris immune signaling molecules 1″–3′ glycocyclic adenosine diphosphate–ribose (3′cADPR) and histidine conjugated to ADPR (His-ADPR). A third family, Acb5, was found to inhibit cyclic oligonucleotide–based antiphage signaling system (CBASS) immunity by enzymatically degrading its signaling molecule, cyclic guanosine monophosphate–adenosine monosphosphate (3′3′-cGAMP). Structural modeling, crystallographic analyses, and biochemical assays confirmed the computational predictions and explained how these proteins neutralize the bacterial immune signals. Homologs of these antidefense protein families were found encoded in thousands of viral genomes, including in well-studied phages such as T2, T4, and T6, which suggests that manipulation of host immune signaling is a common and evolutionarily conserved viral strategy.

CONCLUSION: Our work introduces a structure-based discovery framework for detecting viral proteins that manipulate host immune signaling, independent of sequence similarity or prior annotation. The identification of previously undescribed families of viral sponges and nucleotide-cleaving enzymes in thousands of phage genomes demonstrates that these counterdefense strategies are pervasive in the phage world. This approach could be used in the future to discover analogous inhibitors in viruses infecting any organism of choice, including eukaryotes. □

*Corresponding author. Email: rotem.sorek@weizmann.ac.il Cite this article as N. Tal *et al.*, *Science* **391**, eaea1761 (2026). DOI: 10.1126/science.aea1761

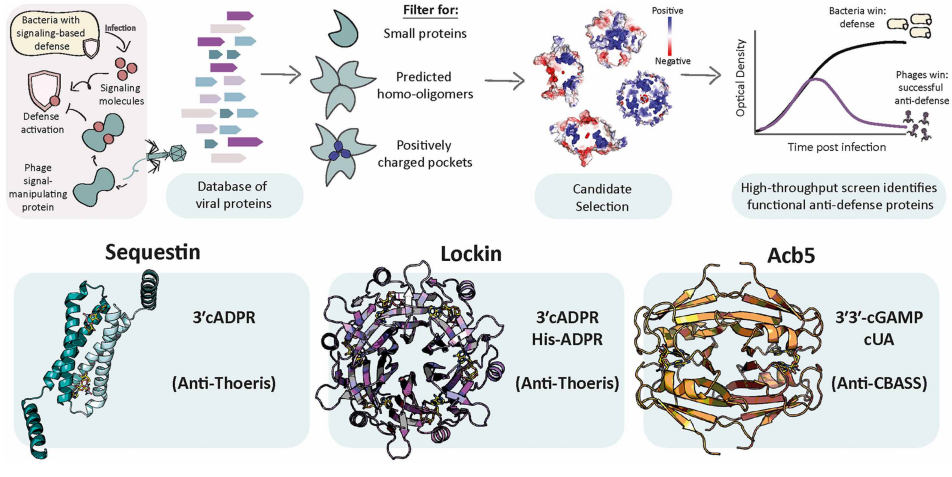

Structure-guided discovery of phage inhibitors of bacterial immune signaling. Small phage proteins of unknown function were modeled using AlphaFold and screened for oligomeric assemblies containing positively charged pockets. Experimental validation revealed three previously uncharacterized protein families: Sequestin and Lockin, sponges that inhibit the Thoeris defense system, and Acb5, an enzyme that cleaves CBASS-produced signals. This study establishes a computational approach for unbiased discovery of immune modulators across phage genomes. cUA, cyclic uridine monophosphate–adenosine monosphosphate.

MICROBIOLOGY

Structural modeling reveals phage proteins that manipulate bacterial immune signaling

Nitzan Tal[1], Romi Hadary[1], Renee B. Chang[2,3], Ilya Osterman[1], Roy Jacobson[4], Erez Yirmiya[1], Nathalie Bechon[1], Dina Hochhauser[1], Miguel López Rivera[2,3], Barak Madhala[1], Jeremy Garb[1], Moshe Goldsmith[5], Tanita Wein[6], Philip J. Kranzusch[2,3,7], Gil Amitai[1], Rotem Sorek[1]*

Immune systems in animals, plants, and bacteria often rely on intracellular nucleotide signaling, which viruses can block by sequestering or degrading these signals. We identified structural and biophysical traits shared by diverse viral antidefense proteins and used these traits to develop a computational pipeline that predicts phage proteins whose role is to manipulate bacterial immune signaling. Experimental validation revealed three previously uncharacterized protein families—Sequestin, Lockin, and Acb5—that inhibit the Thoeris system and the cyclic oligonucleotide–based antiphage signaling system (CBASS). Sequestin and Lockin act as nucleotide "sponges," binding 1″–3′ glycocyclic adenosine diphosphate–ribose (3′cADPR) and histidine conjugated to ADPR (His- ADPR), whereas Acb5 cleaves cyclic guanosine monophosphate–adenosine monosphosphate (3′3′-cGAMP) and related molecules. Structural and mutational analyses explain their binding and catalytic mechanisms. Thousands of homologs occur in phage genomes, highlighting the abundance and diversity of viral strategies to subvert nucleotide-based immunity.

Intracellular signaling plays a fundamental role in innate immunity across all domains of life. A diverse set of immune pathways, widespread in animals, plants, and bacteria, use modified nucleotides as immune signals. These pathways typically include a protein that produces the immune signaling molecule once pathogen invasion is detected and another protein (or protein complex) that receives the immune signal and triggers a downstream immune response (*1*–*3*). One such pathway is the human cyclic guanosine monophosphate–adenosine monosphosphate (cGMP-AMP) synthase–stimulator of interferon genes (cGAS-STING) pathway, in which the cGAS protein produces 2′3′ cyclic GMP-AMP (cGAMP) in response to cytosolic DNA, and the STING protein activates immunity once triggered by cGAMP (*4*). The cGAS-STING pathway evolved from a bacterial antiphage defense system called cyclic oligonucleotide–based antiphage signaling system (CBASS) (*5*, *6*). A wide diversity of CBASS systems has been documented in bacteria, each generating a distinct nucleotide immune signal, including cGAMP, cyclic uridine monophosphate (UMP)–AMP (cUA), cyclic UMP-UMP (cUU), cyclic AMP-AMP-GMP (cAAG), and many others (*5*–*9*). Another family of bacterial antiviral defense system, Pycsar, produces the molecules cyclic UMP (cUMP) and cyclic cytidine monophosphate (cCMP) for antiphage immune signaling (*10*).

[1]Department of Molecular Genetics, Weizmann Institute of Science, Rehovot, Israel. [2]Department of Microbiology, Harvard Medical School, Boston, MA, USA. [3]Department of Cancer Immunology and Virology, Dana-Farber Cancer Institute, Boston, MA, USA. [4]Department of Plant and Environmental Sciences, Weizmann Institute of Science, Rehovot, Israel. [5]Department of Biomolecular Sciences, Weizmann Institute of Science, Rehovot, Israel. [6]Department of Systems Immunology, Weizmann Institute of Science, Rehovot, Israel. [7]Parker Institute for Cancer Immunotherapy at Dana-Farber Cancer Institute, Boston, MA, USA. ***Corresponding author. Email: rotem.sorek@weizmann.ac.il**

Toll/interleukin-1 receptor (TIR) domains have also been documented as components of immune signaling systems, particularly in plants and bacteria. In these systems, a protein with a TIR domain senses infection and then produces an immune signaling molecule that contains derivatives of adenosine diphosphate–ribose (ADPR) (*1*, *3*). In bacteria, TIR signaling is used as part of the Thoeris antiphage defense system. Type I Thoeris systems produce the molecule 3′cADPR (*11*) (also called 1′′–3′ gcADPR), type II Thoeris produces a molecule comprising a histidine conjugated to ADPR (His-ADPR) (*12*), and type IV Thoeris systems produce the molecule N7-cADPR (*13*). These molecules act as second messengers, binding an effector protein in the Thoeris pathway to trigger regulated cell death or growth arrest in response to infection. Bacterial Thoeris systems have been proposed to be the ancestors of plant TIR-dependent immune pathways that similarly use ADPR derivatives for immune signaling (*14*).

Because immune signaling pathways are present in a large fraction of bacteria, archaea, plants, and animal species (*1*, *8*), viruses evolved antidefense proteins to eliminate immune signaling molecules from the cell during infection (*15*). Some of these antidefense proteins are enzymes that cleave and inactivate the molecule, including phage-encoded anti-CBASS1 (Acb1) enzymes that cleave cyclic oligonucleotides produced by CBASS systems (*16*) and anti-Pycsar1 (Apyc1) that cleaves cCMP and cUMP to inhibit Pycsar immunity (*16*). Animal poxviruses also encode cGAMP-cleaving enzymes called poxins, which allow virus escape from cGAS-STING immunity (*17*).

A second class of viral proteins that inhibit host immune signaling are called "sponge" proteins. These proteins tightly bind and sequester the immune signaling molecules, preventing them from activating downstream immunity (*11*, *18*–*20*). Sponge proteins were previously discovered in phages, including the Thoeris antidefense 1 (Tad1) and Tad2 sponges that inhibit bacterial Thoeris systems by binding TIR-produced signaling molecules (*11*, *12*, *18*) and Acb2 and Acb4 that bind cyclic oligonucleotides to inhibit CBASS (*19*, *20*). It has recently been shown that some members of the Tad1 and Tad2 protein families can also bind CBASS-derived ligands (*21*).

To date, the identification of viral proteins that target immune signaling molecules has largely depended on serendipity or on experiments with a limited set of viruses (*11*, *18*–*20*). In this work, we identify structural and biophysical features common to viral nucleotide-binding antidefense proteins, which allows the structure-guided discovery of such proteins in large databases of phage genomes. We describe three previously unknown families of antidefense proteins targeting host immune signaling, cumulatively represented in more than 5000 proteins within phage protein datasets. We further characterize the interactions of these proteins with their target molecules using in-depth biochemical and structural analyses, providing a molecular explanation for their ability to efficiently overcome bacterial defenses.

Results

Protein fusion analysis reveals a distinct sponge family

While analyzing known viral proteins that inhibit bacterial immune signaling, we observed that proteins from two well-characterized sponge families, Tad2 and Acb4, are frequently encoded as a single fused protein in phage genomes (Fig. 1A). We hypothesized that fusion of two distinct sponge domains can grant phages the ability to simultaneously block multiple immune signaling molecules using a single protein. Indeed, coexpression of an Acb4-Tad2 fusion protein from *Pasteurella* phage Pm86 with either type I Thoeris or with type I CBASS canceled the ability of both these systems to provide defense against phages (fig. S1, A and B).

Given the common fusions between Tad2 and Acb4, we hypothesized that additional sponge proteins can be discovered on the basis of their tendency to be fused to proteins from known sponge families. We therefore queried the Pfam database (*22*) for protein families of

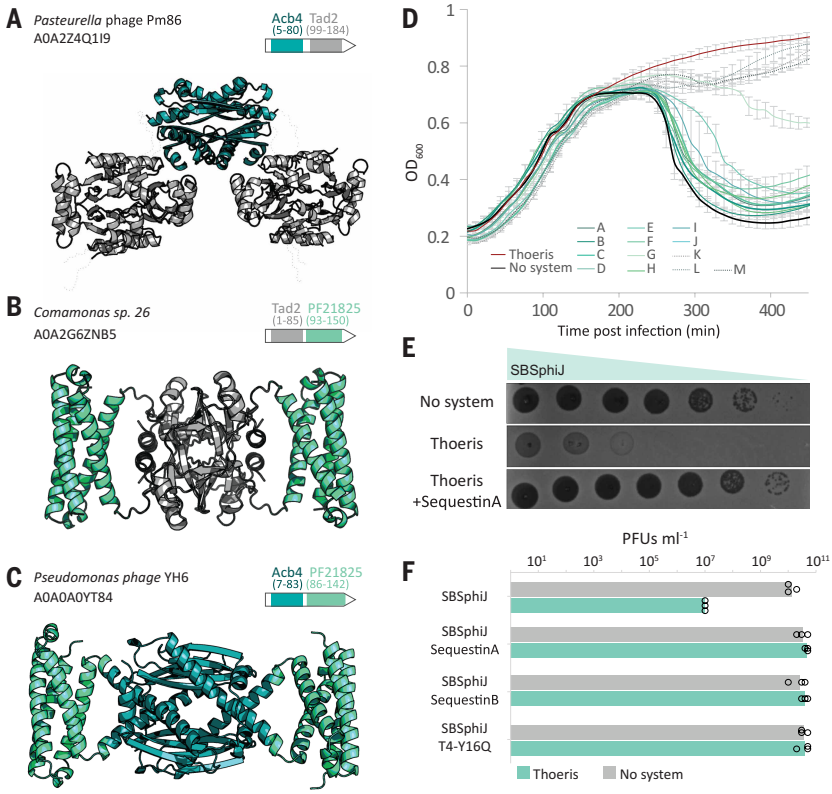

Fig. 1. Proteins with PF21825 domain inhibit type I Thoeris defense. (**A**) A fusion protein of Tad2 and Acb4, found in *Pasteurella* phage Pm86. Each of the Tad2 and Acb4 domains was modeled separately by AlphaFold3 as a homotetramer (Acb4, ipTM = 0.91; Tad2, ipTM = 0.90), and the two models were overlayed. Dashes represent unmodeled linkers between Acb4 and Tad2 domains. (**B**) A fusion protein of Tad2 and a PF21825 domain, detected in a mobile genetic element in *Comamonas* sp. 26. Model of a homo-tetramer, ipTM = 0.74. (**C**) A fusion protein of PF21825 domain and Acb4 from *Pseudomonas* phage YH6. Model of a homo-tetramer, ipTM = 0.74. (**D**) Growth curves of *B. subtilis* cells expressing the type I Thoeris system alone (red), or coexpressing the Thoeris system and a gene with PF21825 Pfam domain (A to M represent the 13 tested PF21825 genes; shades of turquoise and gray), or a control strain without a defense system (black), infected by phage SBSphiJ at an MOI of 0.01. Each curve is the average of three replicates, with error bars indicating standard deviations. (**E**) A representative PF21825 protein (SequestinA, name explained below) that cancels Thoeris defense. Shown are 10-fold serial dilution plaque assays, comparing the plating efficiency of phage SBSphiJ on bacteria that express the type I Thoeris defense system alone or coexpressing the Thoeris system with SequestinA. The control strain lacks the system and expresses GFP instead. Images are representative of three replicates. Data for three replicates for each of the Sequestin genes are presented in fig. S1G. (**F**) Phages engineered to express PF21825 genes overcome Thoeris defense. Shown are data for wild-type SBSphiJ phage as well as SBSphiJ knocked-in with members of the PF21825 Sequestin family. Data represent plaque forming units (PFUs) per milliliter of phages infecting control cells (no system) or cells expressing the type I Thoeris system. Data are averages of three biological replicates with individual data points overlaid.

unknown function that appear fused to either Tad2 (Pfam PF11195) or Acb4 proteins (PF13876). Tad2 was most commonly fused to proteins from Pfam family PF21825 (60 fusion instances). PF21825 was also the most common family fused to Acb4 proteins (91 fusion instances) (Fig. 1, B and C).

PF21825 is a family of short (~60 to 80 amino acids) proteins of unknown function predicted to adopt an α-helical structure (Fig. 1, B and C). Most proteins with this family annotation appear in phage genomes or within prophages in bacterial genomes, which suggests that they primarily carry out a phage-specific function (*22*). Despite frequent fusions with Tad2 and Acb4, proteins with the PF21825 domain most commonly appear as stand-alone proteins that do not contain other detectable domains except for PF21825 (*22*). Based on the preferential presence in phage genomes and frequent fusion with known sponges, we suspected that Pfam PF21825 represents a previously uncharacterized family of viral sponges.

To test whether standalone PF21825 proteins can inhibit bacterial immune signaling, we synthesized and cloned 13 diverse members of this family that are not fused to other protein domains and coexpressed each member with five distinct defense systems, each producing a different immune signaling molecule. These included type I Thoeris from *Bacillus cereus* MSX-D12 (producing 3′cADPR) (*23*), type II Thoeris from *Bacillus amyloliquefaciens* Y2 (*23*) (His-ADPR), type I CBASS from *Escherichia albertii* MOD1-EC1698 (3′3′-cGAMP) (*7*), Pycsar from *Escherichia coli* E831(cCMP) (*10*), and Pycsar from *Bacillus* sp. G1 (speculated to produce cUMP).

We then challenged each strain with phages whose infection is naturally blocked by the respective defense system. Of the 13 PF21825 candidates tested, 10 affected the function of type I Thoeris, inhibiting it either partially or fully. This was observed both through infection in liquid cultures with low multiplicity of infection (MOI), where cultures expressing PF21825 proteins collapsed despite also expressing the Thoeris system (Fig. 1D and fig. S1, C to F), and through plaque assays, showing that coexpression of PF21825 proteins with the Thoeris system rendered the system inactive (Fig. 1E and fig. S1G). To test whether these proteins can inhibit defense also when expressed directly from the genome of the infecting phage, we engineered three of them into the genome of phage SBSphiJ under the control of the native promoter of the *tad1* sponge gene (*11*). SBSphiJ fully overcame this defense system when expressing either of the three PF21825 proteins (Fig. 1F). These results verify that PF21825 represents a family of phage-encoded Thoeris inhibitory proteins. None of the other tested defense systems were inhibited by the 13 members of the PF21825 family that we experimented with (fig. S1, C to F).

The TIR domain protein of type I Thoeris (ThsB) produces 3′cADPR in response to phage infection. This signaling molecule activates the effector protein of the system (ThsA), which then cleaves nicotinamide adenine dinucleotide (NAD^+) and depletes it from the infected cell. To determine whether PF21825 proteins interfere with 3′cADPR signaling, we incubated purified ThsA with lysates from phage-infected cells that express ThsB with or without proteins from the PF21825 family. As was previously shown (*11*, *24*), lysates from infected cells expressing ThsB triggered the NAD^+ glycohydrolase (NADase) activity of ThsA, confirming that the TIR protein ThsB produces 3′cADPR during infection by phage SBSphiJ (Fig. 2A). By contrast, lysates from infected cells coexpressing ThsB together with proteins from the PF21825 family failed to activate ThsA, which suggests that 3′cADPR signaling was impeded in these cells (Fig. 2A).

To test whether PF21825 proteins may bind the signaling molecule of type I Thoeris, we purified a PF21825 protein and performed size exclusion chromatography (SEC) of this protein before and after incubation with 3′cADPR. This experiment revealed an elevated 260 nm/280 nm light absorbance value for the protein preincubated with 3′cADPR, which indicates that the protein directly binds the immune signaling nucleotide (Fig. 2B). After incubation of the purified protein in a 1:1 ratio with 3′cADPR, the molecule was

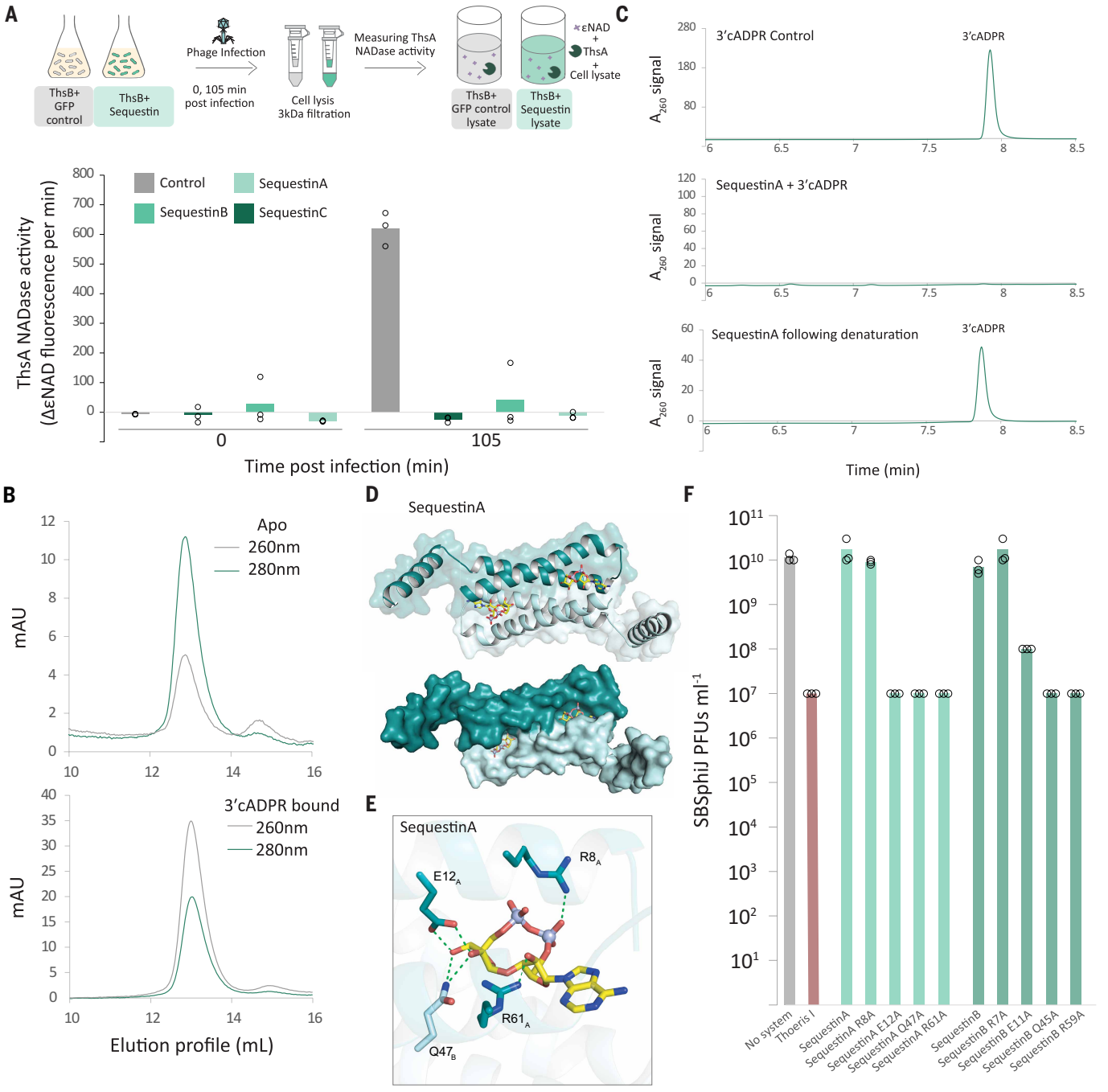

Fig. 2. Sequestin is a family of viral sponges that bind and sequester 3′cADPR. (**A**) Sequestin proteins prevent accumulation of 3′cADPR in Thoeris-expressing infected cells. Cells expressing ThsB from *B. cereus* MSX-D12, or coexpressing both ThsB and genes from the Sequestin family, were infected with the phage SBSphiJ at an MOI of 10. Cell lysates were extracted before infection ($t = 0$) and 105 min after infection and were filtered to retain small molecules. Filtered lysates were then incubated with ThsA, and the NADase activity of ThsA was measured using a nicotinamide 1,N6-ethenoadenine dinucleotide (εNAD) cleavage fluorescence assay. Bars represent the means of three experiments, with individual data points overlaid. Control represents experiments with lysates from cells expressing GFP together with ThsB. (**B**) SEC of SequestinA in apo state or after incubation with 3′cADPR. Light absorbance values at 260 nm and 280 nm are shown. (**C**) HPLC analysis of 3′cADPR incubated with either buffer (control; top lane) or with purified SequestinA (middle lane) at 1:1 ratio. Bottom lane shows the molecule release after the molecule-bound SequestinA was denatured by chloroform. (**D**) Structure of the AlphaFold3-predicted complex formed by a homodimeric unit of SequestinA, together with 3′cADPR. Cartoon and surface representations are shown. (**E**) Close-up view of the predicted interactions of 3′cADPR with SequestinA from the model shown in (D), highlighting key interacting residues. (**F**) Effect of point mutations in SequestinA and SequestinB on the ability of the sponge to cancel the defensive activity of type I Thoeris. Data represent PFUs per milliliter of SBSphiJ phage infecting negative control cells, cells expressing Thoeris, or cells coexpressing Thoeris and a sponge variant. Average of three replicates with individual data points overlaid.

completely depleted from the solution, as confirmed by high-performance liquid chromatography (HPLC) (Fig. 2C). Furthermore, chloroform denaturation of the 3′cADPR-bound protein released intact 3′cADPR molecules back into the medium (Fig. 2C). These results demonstrate that the studied protein is a viral sponge that binds and sequesters 3′cADPR to counteract Thoeris immunity.

Previously discovered families of viral sponge proteins were named after the defense systems that the founding member of the family was first shown to inhibit. Thus, as the first sponges to be discovered inhibited Thoeris defense, they were called Thoeris antidefense 1 and 2 (Tad1 and Tad2) (*11*, *18*). However, later studies have shown that some members of the Tad1 and Tad2 sponge families can bind CBASS-produced signaling molecules (*21*). To avoid ambiguous naming, we denote the PF21825 family of sponges with the name Sequestin. Because most Sequestin proteins that we experimented with were derived from metagenomic databases of uncharacterized viruses, in this work, we refer to metagenome-derived protein members of this family by the names SequestinA, SequestinB, and so on.

To gain deeper insight into the molecular mechanism by which Sequestin sponges sequester the immune signaling molecule, we modeled members of this sponge family using AlphaFold3 in the presence of 3′cADPR at various oligomeric states (Fig. 2D and fig. S2A). These proteins were predicted with high confidence to be folded as homo-dimers or homo-tetramers (fig. S2, A and B). In the homo-dimeric form, the two protomers are organized in an antiparallel manner. Two symmetrical, elongated pockets are formed in the interface between protomers, and AlphaFold3 places 3′cADPR in these pockets with high confidence (Fig. 2D and fig. S2A). Despite substantial sequence divergence between the Sequestin proteins that we modeled, AlphaFold3 consistently places 3′cADPR in the same orientation within the Sequestin binding pockets, with high interface-predicted template modeling (ipTM) and predicted local difference distance test (pLDDT) confidence scores, implying that this placement reflects natural binding. In the homo-tetrametic form, two homo-dimers are positioned back-to-back (fig. S2B). Mass photometry analysis of SequestinA suggests that this protein purifies as a tetramer in solution (fig. S2B).

We focused on protein SequestinA to further study the molecular interactions between the sponge and 3′cADPR. The model predicts that the placement of the immune signaling molecule in the pocket is coordinated through interactions with multiple conserved side chains. The adenine-proximal and adenine-distal ribose moieties are contacted by R61 and E12 of protomer 1, respectively, and the short distance between the amino acid side chains and the hydroxyl groups of the respective riboses suggests hydrogen bonding (Fig. 2E). Q47 from the second protomer is also predicted to contribute to the interaction with the adenine-distal ribose (Fig. 2E). The phosphate groups are in close vicinity to the NH_2 group of R8, suggesting that this residue coordinates the placement of the phosphates in the pocket. All residues indicated above are conserved in diverse members of the Sequestin sponge family and were predicted to interact with the signaling molecule also in other members of the Sequestin family, which further supports that they play a role in the interactions with 3′cADPR (fig. S2C). Substituting each of E12, Q47, or R61 into alanine resulted in loss of antidefense activity, but an R8A (Arg^8→Ala) substitution did not (Fig. 2F and table S1). Mutations in the corresponding residues in SequestinB—R7, E11, Q45, and R59A—resulted in the same phenotypes (Fig. 2F).

Using Foldseek (*25*) and sequence-based analyses, we detected 3244 proteins belonging to the Sequestin sponge family in the IMG/VR v4 database of viral proteins (*26*) (table S2). Further analysis in a database of ~25,000 fully sequenced phage genomes (*27*) found these sponges in 639 phages, including phages infecting organisms belonging to 40 taxonomic genera from six bacterial phyla and one archaeal phylum (table S2). Sequestin sponges were detected in the genomes of 14 phages from the BASEL collection (*28*), all of which belong to the Tevenvirinae group. Notably, some well-studied model phages, including phages T2, T4, and T6, encode a protein from the Sequestin family. In phage T4, this protein is called Y16Q, a 64–amino acid–long protein of unknown function. AlphaFold3 modeling showed that Y16Q folds as a homo-dimer with two pockets predicted to bind 3′cADPR, which suggests that this T4 protein can inhibit Thoeris similar to other members of the sponge family (fig. S2A). Indeed, engineering Y16Q into phage SBSphiJ under the control of the *tad1* native promoter (*18*) rendered the phage resistant to Thoeris, demonstrating that the phage T4 Y16Q protein is an anti-Thoeris sponge (Fig. 1F). Together, these results show that Sequestin is an anti-Thoeris sponge family abundant and widespread in phages in nature.

Computational prediction of viral proteins that counter immune signaling

Examining the predicted structures of Sequestin sponges, as well as the determined crystal structures of other known sponges (*11*, *18*–*20*), we noticed that they all share common biophysical properties. First, all sponges are encoded by short proteins (often <100 amino acids in size), and in all cases, the ternary structure comprises a homo-oligomer—homo-dimers in the case of Sequestin, homo-tetramers in the case of Acb4 and Tad2, or homo-hexamers for Tad1 and Acb2. In all cases, the pockets that sequester the immune signaling molecules are formed at the interfaces between protomers so that the final complex contains multiple binding sites for target molecules [up to eight sites in the case of Tad1 (*21*)]. This distinctive protein complex organization allows phages to encode multimolecule binding sponges while devoting little genomic space for this purpose.

Further analysis of crystal structures and AlphaFold predictions of known sponges in their apo forms showed that, in almost all cases, the nucleotide binding pockets are deeply engraved or form large void spaces in the protein (Fig. 3A). These spaces typically have an inner surface area of 200 to 700 $Å^2$ and are almost always highly positively charged, likely to accommodate interactions with the negative charge of the phosphate groups that are present in all known nucleotide signaling molecules (Fig. 3A). Given that known sponge proteins display the same biophysical traits despite belonging to evolutionarily unrelated families, we reasoned that additional unknown families of viral sponges can be discovered on the basis of structure-guided analyses of large viral protein databases. Under the premises of this hypothesis, short viral proteins that form homo-oligomers, in which multiple positively charged pockets are formed at the interface between protomers, can be candidate sponges.

To test this hypothesis, we examined a dataset of roughly 32 million nonredundant proteins derived from ~2 million phage genome scaffolds found in the IMG/VR v3 database, as previously described (Materials and methods) (*29*, *30*). Proteins were clustered on the basis of sequence similarity, excluding those with known functional annotations as well as those larger than 200 amino acids. A representative sequence from each cluster was analyzed using AlphaFold-Multimer (*31*) to examine the likelihood of the protein to form dimeric, trimeric, tetrameric, pentameric, or hexameric homo-oligomers. We then searched for pockets with internal surface areas sized 100 to 1000 $Å^2$ within high-confidence homo-oligomeric predicted structures using the pocket prediction tools CastP and AutoSite (*32*, *33*) and retained predicted structures in which multiple pockets were formed in the interfaces between protomers and in which the internal surfaces of the pockets were positively charged (Materials and methods) (Fig. 3B). On the basis of these parameters, we prioritized a set of >120 candidate proteins for further experimentation. Although the selected proteins fulfill the theoretical structural constraints of sponges, we expect that only a minority of them represent real sponge proteins because positively charged pockets can have roles in the manipulation of nonimmune nucleotides (*34*, *35*) as well as other roles (*36*, *37*).

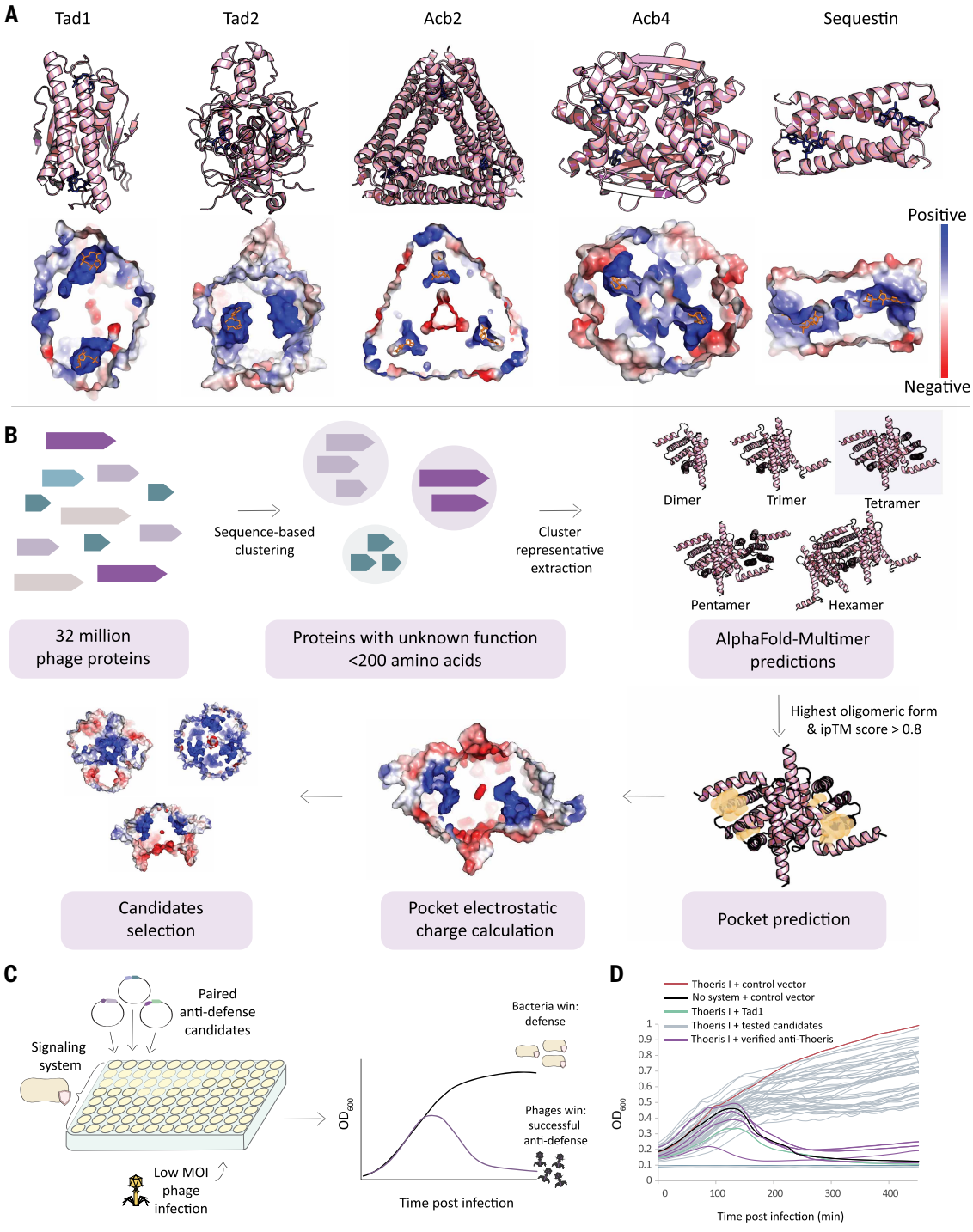

Fig. 3. A structure-guided computational and experimental pipeline for the discovery of viral proteins that manipulate immune signaling. (**A**) Crystal structures of Tad1, Tad2, and Acb2 (PDB: 7UAW, 8SMG, and 8IY2, respectively) and AlphaFold3-predicted structures for Acb4 (uniport accession: A0A0B3RSW4, ipTM = 0.93), and SequestinB (ipTM = 0.94), together with their respective ligands. Cross sections into the proteins are presented, with surface as an electrostatic map in a blue-red scale. Blue blebs represent positively charged pockets within the proteins. A dimer unit of the Tad1 hexamer is presented for clarity. Solved or AlphaFold-predicted structures were modeled with their respective ligands. (**B**) A computational pipeline to predict viral proteins that interact with host immune signals. The phage protein space is clustered, and representative proteins are selected from clusters of short proteins of unknown function. High-scoring AlphaFold-Multimer predictions for homo-oligomers are analyzed by CastP (*32*) and Autosite (*33*) to identify pockets with sizes typical to those found in known sponge proteins. Proteins with positively charged pockets are further evaluated as possible antidefense proteins. (**C**) Schematic of the experimental setup. Liquid cultures of bacteria harboring the defense system are grown in a 96-well plate format. Each well is transformed with a different plasmid that expresses a pair of antidefense candidates, with antibiotics added to select for cells that acquired the plasmid. Bacteria are subsequently infected with phages in a low MOI, and optical density (OD) is measured to identify successful phage infections. (**D**) An example of an infection assay described in (C). Cells expressing the type I Thoeris system from *B. cereus* MSX-D12 were infected with phage SBSphiJ at MOI of 0.01. Each curve represents growth of bacteria transformed with a pair of candidate antidefense genes, with negative control cells transformed with a plasmid expressing GFP (black), and positive control cells transformed with a plasmid expressing Tad1 (green). Purple curves represent cases where the transformed plasmid allowed the phage to propagate and cause eventual culture collapse, suggesting that one of the genes in the transformed plasmid inhibited Thoeris defense.

We developed a high-throughput screening methodology to test the effect of 124 selected candidates on multiple defense systems. In this method, pairs of candidate sponges are expressed as a two-gene operon from a plasmid that is introduced into bacterial strains in which a defense system was genomically integrated (Fig. 3C and Materials and methods). This procedure takes place in a 96-well plate format where candidate or control plasmids are transformed. The cultures are grown and passaged to fresh media under antibiotic selection to maintain the plasmid, and then the culture is subjected to phage infection in liquid media at low MOI. This approach identifies proteins that, when coexpressed with the defense system, cancel its activity and allow phage propagation and phage-mediated culture collapse (Fig. 3C). The benefit of this method is that it does not necessitate isolation of individual transformed colonies, which would have made the screen of >120 candidates versus multiple defense systems prohibitively labor intensive; the drawbacks are that only ~80% of the attempted transformations were successful in the 96-well plate format and that positive hits necessitate further verification (table S3).

We used this method to transform 62 plasmids, each expressing a pair of candidate genes, to the five bacterial strains expressing the signaling defense systems type I Thoeris, type II Thoeris, CBASS, Pycsar (cCMP), and Pycsar (cUMP) and infected transformants with phages naturally restricted by the respective defense system (Fig. 3, C and D). In cases where culture collapse was observed with at least one of the defense systems, the two genes in the pair were separated, and each gene was individually tested for its ability to inhibit the respective defense system using plaque assays (table S3). Nine proteins were verified as exhibiting substantial antidefense activity and were further investigated through biochemical assays (see below). Seven of them were found to directly interact with immune signaling molecules, and these were grouped into two distinct protein families that are further studied in detail below (table S3).

Lockin, a sponge family that inhibits type I and type II Thoeris

Lockin is a large family of proteins predicted to fold into curved, elongated structures mostly comprising β sheets (fig. S3A). AlphaFold-Multimer consistently predicts these proteins to fold into symmetrical, cog-like hexamers, with each monomer comprising a symmetrical segment of the cog (fig. S3, B and C). Positively charged pockets are formed between the segments, and these pockets are enclosed by a loop that emanates from one of the protomers (fig. S3, C and D). The surface areas of the predicted pockets range between ~260 and 440 Å^2, within the premises of the sizes of pockets in known sponges (table S4). Mass photometry analysis of a purified protein verified that it purifies as a hexamer, confirming the oligomeric structure prediction of AlphaFold (fig. S3E).

Four Lockin proteins in our set exhibited strong activity against type I Thoeris (Fig. 4, A to C), and two of them also inhibited type II Thoeris when coexpressed with the system (Fig. 4D). One additional Lockin protein exhibited activity against type II Thoeris exclusively (Fig. 4D). Engineering of Lockin proteins into phage SBSphiJ under the native promoter of *tad1* resulted in a phage resistant to one or both of the tested Thoeris systems (Fig. 4E), consistent with the coexpression results. Coexpression of Lockin proteins in phage-infected cells that express ThsB rendered the cells devoid of detectible 3′cADPR (Fig. 4F), similar to the results obtained for the anti-Thoeris sponge Sequestin (Fig. 2A). These results verify that Lockin is a family of anti-Thoeris proteins.

To further examine the interaction between Lockin and the signaling molecule, we purified the Lockin protein LockinA and incubated it with 3′cADPR. SEC followed by HPLC analysis showed an elevated 260 nm/280 nm absorbance ratio for the protein that had been preincubated with 3′cADPR, which suggests that it binds the signaling molecule (fig. S3F). 3′cADPR was eliminated from the solution after incubation with the Lockin protein and reappeared after heat denaturation of the LockinA–3′cADPR complex (Fig. 4G). Together, these results verify that Lockin is a family of anti-Thoeris sponges.

To define the molecular basis of Lockin anti-Thoeris immune evasion, we determined a 1.6-Å x-ray crystal structure of LockinA in complex with 3′cADPR (Fig. 4H). Consistent with AlphaFold predictions, Lockin forms a hexameric assembly that sequesters six molecules of 3′cADPR (Fig. 4H). The 3′cADPR binding site resides in a deeply recessed pocket at the interface between adjacent protomers. The 3′cADPR ligand is coordinated by nucleobase-specific interactions between the adenine base and residue T47 protomer A ($T47_A$) and $Q59_B$ that read out the N1 and N6 positions of the nucleobase Watson-Crick edge (Fig. 4, I and J). On the nucleobase Hoogsteen edge, Lockin residue $K48_B$ makes further contacts with the nucleobase and coordinates the adenine N7 position (Fig. 4, I and J). In addition to base-specific contacts, multiple Lockin residues stabilize the diphosphate backbone of 3′cADPR, including a network of polar contacts from $K45_A$, $K35_B$, $S46_B$, and $K48_B$ (Fig. 4, I and J). Point mutations in either K45 or K48 abolished or reduced the antidefense activity of LockinA, as demonstrated by partial or complete restoration of immunity in cells coexpressing Thoeris and the mutated sponge (Fig. 4K and table S1). Mutating T47 did not change the antidefense phenotype.

We detected 907 sequence and structural homologs of the verified Lockin proteins in the IMG/VR v4 database of viral proteins (*26*) (table S5). Analyzing homologs from isolate genomes, we found that Lockin proteins appeared in phages infecting bacteria from 11 taxonomic genera, including *Bacillus*, *Rosebium*, *Pseudovibrio*, *Dehalobacter*, *Microcystis*, and *Cohnella* (table S5). In all cases, the proteins were annotated as phage proteins of unknown function, with no known domain annotation. We were not able to find members of this family within full-length sequenced and assembled phage genomes in the INPHARED database (*27*), which indicates that these proteins are underrepresented in model phages whose genomes were fully sequenced.

Acb5, a family of phage proteins that inhibit CBASS

Two phage proteins in our screen were able to inhibit the activity of the 3′3′-cGAMP–producing CBASS operon from *E. albertii* (Fig. 5, A to C). Both these proteins, when coexpressed with the signal-producing cGAS/DncV-like nucleotidyltransferase (CD-NTase) enzyme of the *E. albertii* CBASS, prevented the accumulation of 3′3′-cGAMP in phage-infected cells (Fig. 5D). Despite low sequence similarity between the two proteins (fig. S4, A and B), both proteins are predicted to fold into structurally similar homo-tetrameric complex by AlphaFold-Multimer with high confidence (Fig. 5, E and F). Two large, positively charged pockets with internal surface areas of 425 to 530 Å^2 are formed between loops at the interface between pairs of protomers (Fig. 5G). We refer to this family of proteins as Acb5 (anti-CBASS 5).

Thin-layer chromatography (TLC) analysis showed that incubation of purified Acb5 with radiolabeled 3′3′-cGAMP resulted in altered migration of the radiolabeled signal, leading us to suspect that Acb5 proteins may degrade cGAMP (Fig. 6A). To investigate this hypothesis, we incubated purified Acb5A with cGAMP and analyzed the resulting samples using HPLC. The analysis revealed that cGAMP was enzymatically digested into two distinct products (Fig. 6, B and C). Further analysis using HPLC and mass spectrometry showed that the degradation products had mass/charge ratio (m/z) values and retention times identical to those of standard 2′3′-cyclic AMP (cAMP) and 2′3′-cyclic GMP (Fig. 6, C and D, and fig. S4, C and D), which suggests that Acb5A cleaves cGAMP in two places and leaves 2′3′ cyclic phosphate groups on the cleavage products.

Incubation of Acb5A with 3′3′-cUA also resulted in partial degradation of cUA, which suggests that Acb5A can use 3′3′-cUA as a substrate but to a lower efficiency compared with cGAMP (Fig. 6, E and F). HPLC and mass spectrometry analyses showed that the major degradation product has an m/z value identical to that of cUA but with a different retention time, suggesting that this product is the outcome of a single

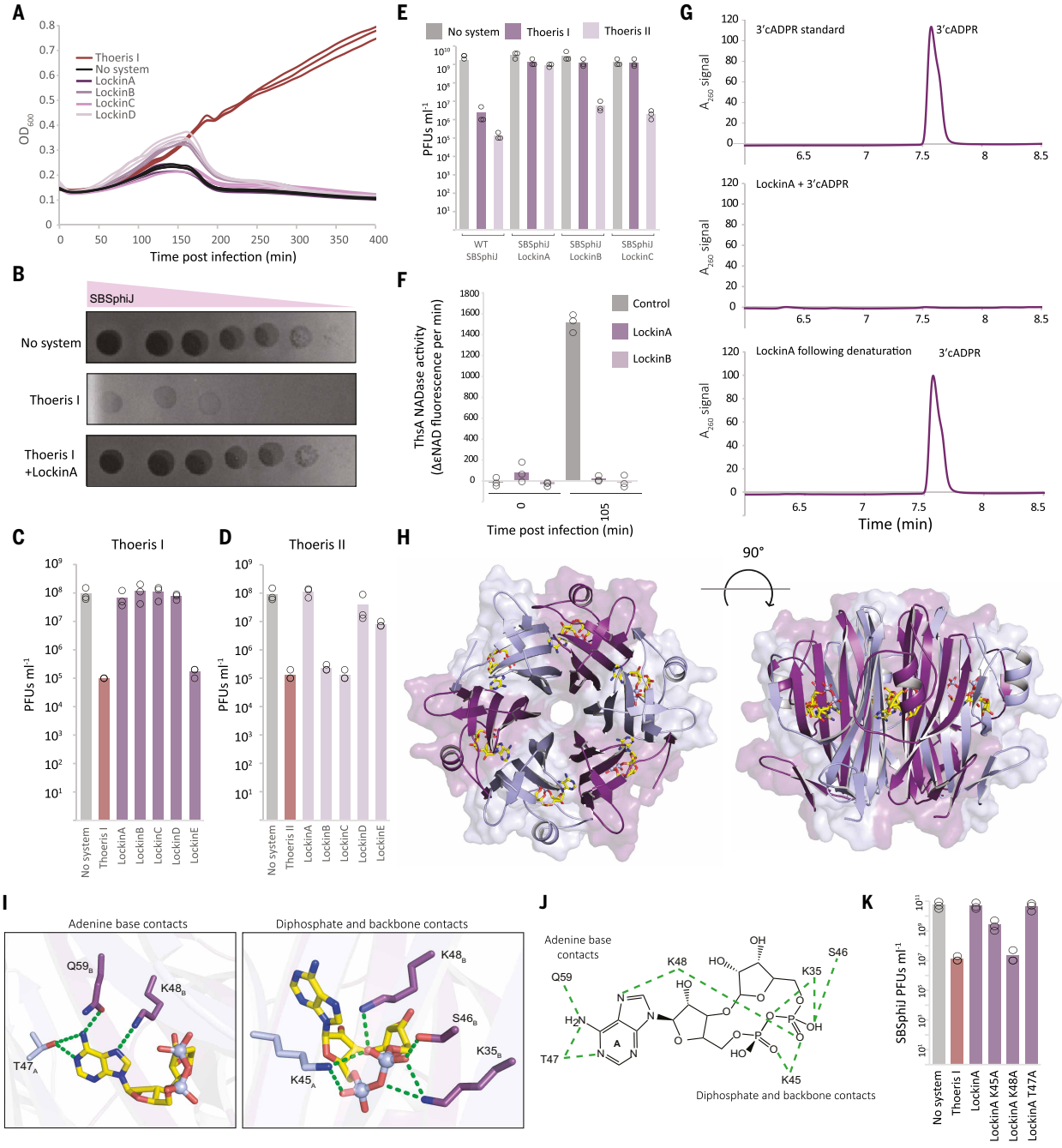

Fig. 4. Lockin is a family of phage proteins that inhibit Thoeris defense. (**A**) Growth curves of *B. subtilis* cells expressing type I Thoeris from *B. cereus* MSX-D12 (red), or coexpressing type I Thoeris and a Lockin protein (shades of purple), or control cells expressing GFP instead of the Thoeris system (black). Cells were infected with SBSphiJ phage at an MOI of 0.01. Results of three experiments are presented as individual curves. (**B**) A representative Lockin protein (LockinA) capable of overcoming type I Thoeris defense. Shown are 10-fold serial dilution plaque assays, comparing the plating efficiency of phage SBSphiJ on bacteria that express the type I Thoeris alone or with LockinA. Images are representative of three replicates. (**C**) Plating efficiency of phage SBSphiJ on negative control cells, cells expressing type I Thoeris, and cells expressing both type I Thoeris and a Lockin gene. Data represent PFUs per milliliter, and bars show the average of three replicates with individual data points overlaid. (**D**) Same experiment as in (C), but with type II Thoeris from *B. amyloliquefaciens* Y2. (**E**) Phages engineered to express Lockin genes overcome defense of type I and type II Thoeris. Shown are data for wild-type SBSphiJ phage, as well as SBSphiJ knocked-in with members of the Lockin family. Data represent PFUs per milliliter of phages infecting control cells (no system), or cells expressing a type I or II Thoeris system. Average of three biological replicates with individual data points overlaid. (**F**) Lockin proteins prevent accumulation of 3′cADPR in Thoeris-expressing infected cells. Legend is as in Fig. 2A. (**G**) HPLC analysis of 3′cADPR incubated with either buffer (control; top lane) or with purified LockinA (middle lane) at 1:1 ratio. Bottom lane shows the molecule release after the molecule-bound Lockin was denatured in 98°C for 10 min. (**H**) Crystal structure of LockinA in complex with 3′cADPR. (**I**) Detailed view of LockinA residues that interact with the 3′cADPR adenine base and diphosphate backbone. Green dashed lines indicate hydrogen bonding interactions. Subscript denotes individual protomers within the Lockin hexamer. (**J**) A two-dimensional (2D) map presenting a detailed view of 3′cADPR adenine base and diphosphate backbone and their LockinA residues interactions. (**K**) Effect of point mutations in LockinA on the ability of the sponge to cancel the defensive activity of type I Thoeris. Data represent PFUs per milliliter of SBSphiJ phage infecting negative control cells, cells expressing Thoeris, or cells coexpressing Thoeris and a sponge variant. Average of three replicates with individual data points overlaid.

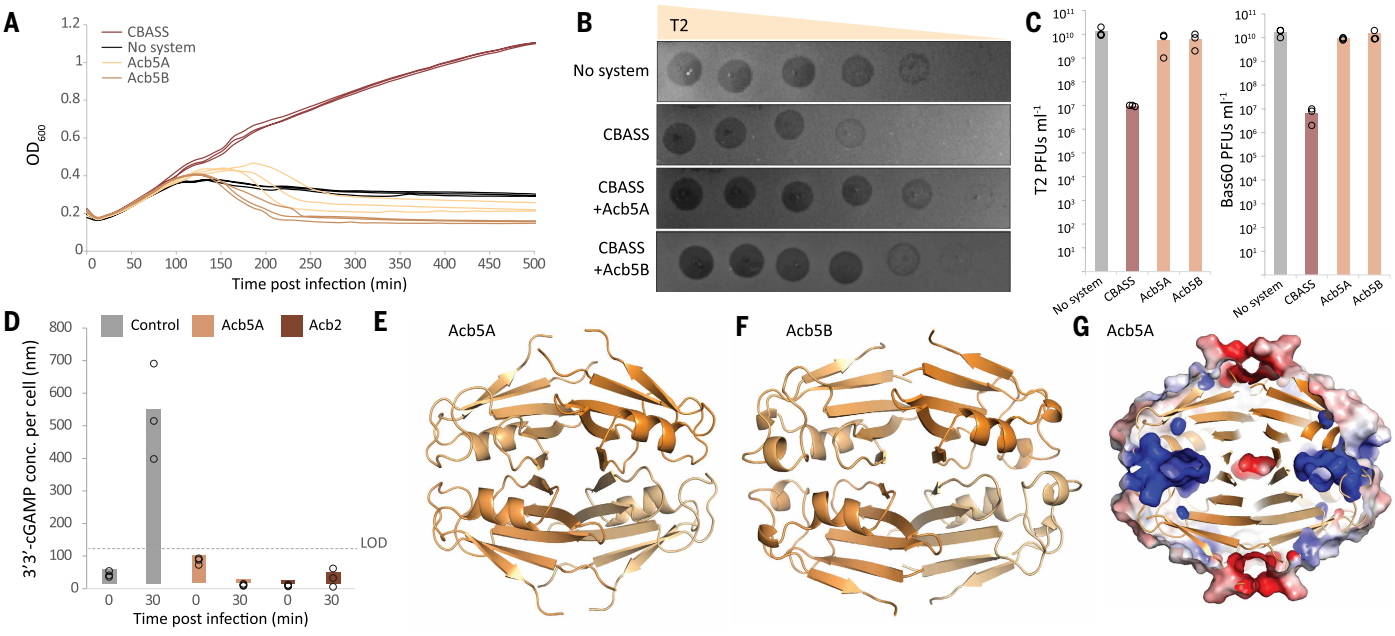

Fig. 5. Acb5 proteins inhibit CBASS signaling. (**A**) Growth curves of *E. coli* cells expressing either a genomically integrated CBASS system from *E. albertii* MOD1-EC1698 (red), coexpressing CBASS and Acb5 proteins (shades of orange), or negative control cells lacking the system (black), infected with T2 phage at an MOI of 0.001. Results of three experiments are presented as individual curves. (**B**) Acb5 is capable of overcoming CBASS defense. Shown are 10-fold serial dilution plaque assays, comparing the plating efficiency of T2 on bacteria that express the CBASS defense system, or bacteria coexpressing CBASS with Acb5 proteins, or a control strain that lacks the system. Images are representative of three replicates. (**C**) Plating efficiency of phage T2 and phage Bas60 on negative control cells, cells expressing CBASS, and cells expressing both CBASS and an Acb5 gene. Data represent PFUs per milliliter, and bars show the average of three replicates with individual data points overlaid. (**D**) Acb5 prevents cGAMP accumulation in infected cells. Cells expressing the CD-NTase enzyme of the *E. albertii* CBASS, or coexpressing the CD-NTase and Acb5A, were infected with the phage Bas60 at an MOI of 10. Cell lysates were obtained before infection (0 min) and during infection (30 min) and filtered to retain small molecules. cGAMP concentration in filtered lysates was measured using a 3′3′-cGAMP ELISA kit, and cGAMP concentration per cell was calculated based on estimated cell counts. Cells coexpressing CBASS and Acb2 (*19*) were used as positive control. Bars represent the means of three experiments, with individual data points overlaid. Limit of detection is presented as a dashed line. (**E** and **F**) AlphaFold3-predicted tetramer complex for Acb5A (ipTM = 0.89) (E) and Acb5B (ipTM = 0.88) (F). Protomers are presented in different shades of orange. (**G**) Cross section in the AlphaFold3-predicted tetramer complex for Acb5A with surface displayed as an electrostatic map (blue-red scale for positive-negative charges). Blue blebs represent positively charged pockets within the protein.

cleavage and phosphate cyclization event (Fig. 6F). We hypothesize that cleavage takes place in the adenine moiety, implying a specificity of Acb5A for purines as substrates. These findings indicate that Acb5 is a family of enzymes that degrade CBASS-derived signaling molecules, thus inhibiting CBASS by disrupting immune signaling cascade.

AlphaFold3 consistently placed 3′3′-cGAMP, as well as the catalysis products 2′3′-cyclic AMP (cAMP) and 2′3′-cyclic GMP (cGMP), within the predicted pockets (Fig. 6G). The ligand-binding pocket is predicted to be symmetric and is formed by conserved residues from two adjacent protomers (Fig. 6H). The model predicts the conserved residue W38 from both protomers to interact with the adenine and guanine bases by π-π stacking. R10 and H61 are both predicted to interact with the phosphate moieties, and R10 is also placed in close proximity to the ribose moieties. Mutating either of these residues eliminated the antidefense activity of Acb5A, supporting their predicted roles in the interaction with cGAMP (Fig. 6I and table S1).

We detected 1480 homologs of Acb5 proteins in the IMG/VR v4 database of viral proteins (*26*) based on sequence and structural homology analyses (table S6). Analyzing homologs from isolate genomes showed an extensive taxonomic diversity, with Acb5 proteins appearing in phages infecting both bacteria and archaea belonging to more than 20 taxonomic genera (table S6). Acb5 proteins were especially abundant in phages infecting bacteria from the *Actinobacteriota* phylum, including *Streptomyces*, *Mycobacterium*, *Nonomuraea*, and many more (table S6). Analysis of the INPHARED database of completely sequenced phage genomes (*27*) found Acb5 homologs in 96 phage genomes (table S6). Consistent with the observations above, most of the Acb5 homologs in isolate phage genomes were found in phages infecting *Streptomyces* (66 phages) and *Mycobacteria* (14 phages). Homologs of Acb5 were also found in 11 phages infecting *Bacillus* species and five viruses infecting the halophilic archeaeon *Haloarcula* (table S6).

Discussion

In this study, we showed how proteins with counterimmune activities can be discovered within large datasets of viral proteins based on the biophysical characteristics of predicted protein structural models. A major benefit of this approach is that it does not require a priori knowledge about the function of the studied proteins, nor does it necessitate these proteins to be present in model organisms. An example for this is the discovery of Acb5, which is an anti-CBASS enzyme enriched in phages infecting *Streptomyces*, bacterial species not commonly studied in the context of phage-bacteria interactions. Similarly, proteins from the Lockin family were not detected within sequenced genomes of model phages, which demonstrates how unbiased structural analyses of phage proteomes can reveal antidefense proteins underrepresented in known model viruses.

We find it notable that the well-studied phage T4 encodes multiple proteins that inhibit bacterial immune signaling systems. T4 was first found to encode anti-CBASS 1 (Acb1), an enzyme that cleaves and inactivates cyclic dinucleotides and cyclic trinucleotides (*16*). Later

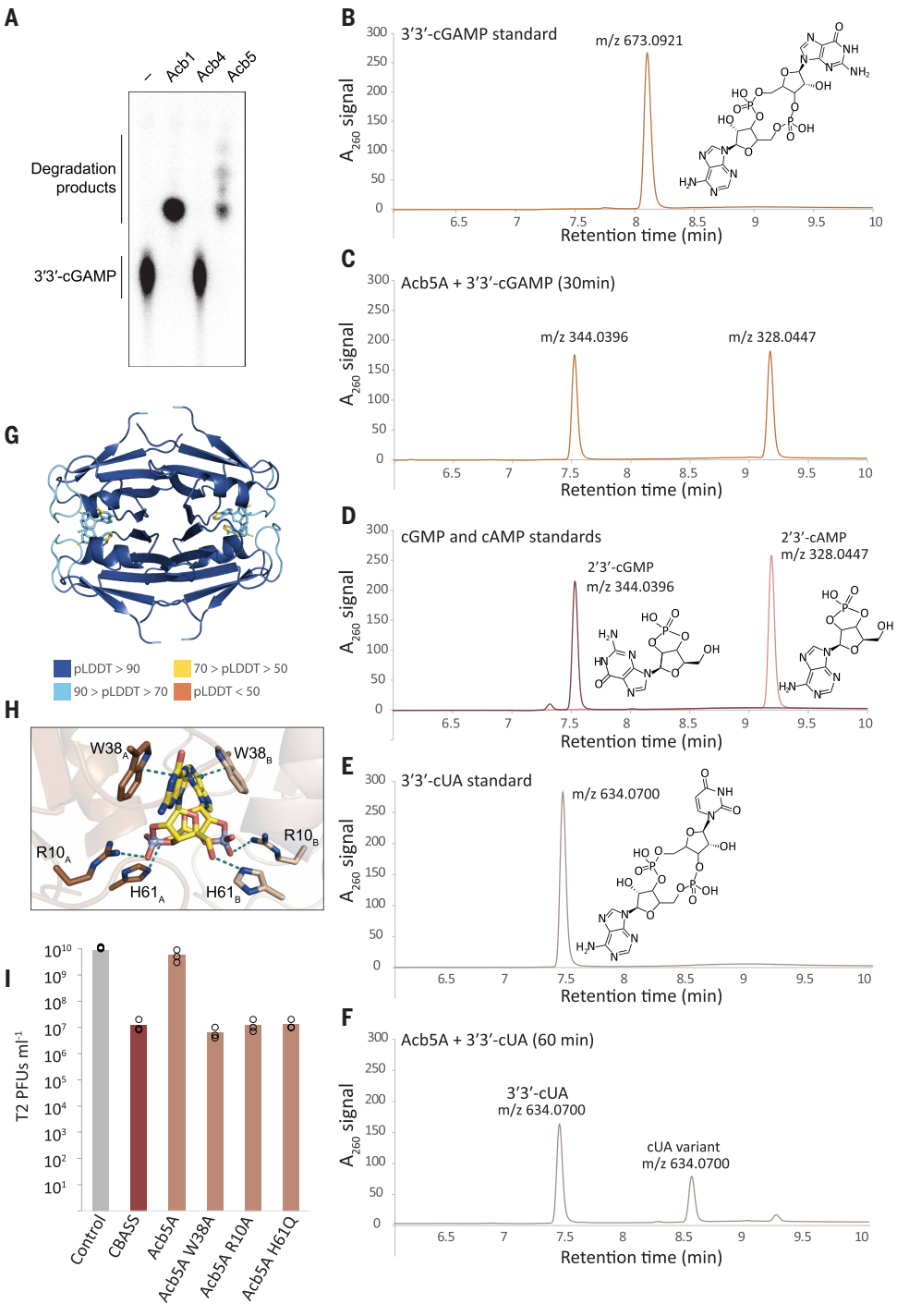

Fig. 6. Acb5 is an enzyme that cleaves CBASS signaling molecules. (**A**) TLC analysis of Acb5A nuclease activity. Recombinant Acb5 was incubated with α-^{32}P–radiolabeled 3′3′-cGAMP, and degradation products were visualized by TLC. Purified Acb1 (an enzyme that cleaves 3′3′-cGAMP) (*16*) and Acb4 (a 3′3′-cGAMP sponge) (*20*) are included as controls. Data are representative of at least three independent experiments. (**B**) HPLC analysis of synthetic 3′3′-cGAMP. The *y* axis represents light absorbance at 260 nm. (**C**) HPLC analysis of degradation products of 3′3′-cGAMP after 30 min incubation with purified Acb5A. *m/z* values, as measured in mass spectrometry, are indicated for each product. Data are representative of three independent experiments. (**D**) HPLC analysis of synthetic 2′3′-cAMP and 2′3′-cGMP standards. (**E**) HPLC analysis of synthetic cUA. (**F**) Degradation products of 3′3′-cUA after 60-min incubation with purified Acb5A. (**G**) AlphaFold3-predicted tetramer complex for Acb5A with 2′3′-cAMP and 2′3′-cGMP (ipTM = 0.87, pTM = 0.90), colors represent pLDDT scores. (**H**) Close-up view of the predicted interactions of 2′3′-cAMP and 2′3′-cGMP with Acb5A from the model shown in (G), highlighting key interacting residues. (**I**) Effect of point mutations in Acb5A on the ability of the enzyme to cancel the defensive activity of CBASS. Data represent PFUs per milliliter of T2 phage infecting negative control cells, cells expressing CBASS, or cells coexpressing CBASS and Acb5A. Average of three replicates with individual data points overlaid.

studies have shown that T4 also encodes anti-CBASS 2 (Acb2), a sponge that sequesters 3′3′-cGAMP (*19*). Our study now shows that T4 also encodes a sponge from the Sequestin family, Y16Q, capable of inhibiting Thoeris defense. The observation that the same phage encodes multiple proteins that counteract diverse immune signaling systems attests to the importance of signaling-based systems in the phage-host arms race.

Through our unbiased approach, we also discovered Acb5 as the founding member of a distinct family of cGAMP-degrading enzymes, demonstrating further functional diversity of phage-encoded nucleases involved with evasion of host immunity. Notably, the Acb5 family does not share structural homology with Acb1 or any other immune evasion phosphodiesterase enzymes, which indicates that phages have evolved multiple proteins for degrading host nucleotide immune signals (*16*, *38*, *39*). In contrast to Acb1, which is a monomeric enzyme that hydrolyzes one bond in 3′3′-cGAMP and releases a linear product, Acb5 forms a twofold symmetric active site that hydrolyzes both phosphodiester linkages in 3′3′-cGAMP and releases mononucleotide products. Together, these observations demonstrate that our unbiased systematic analysis of phage proteomes can be applied to uncover unexpected mechanisms that phages use to subvert host nucleotide immune signaling.

Although our approach is useful for the discovery of previously undescribed sponges and nucleotide-cleaving counterimmune enzymes, it cannot identify all phage sponges and enzymes. For example, Acb1 and Apyc1, enzymes that cleave and inactivate the immune signaling molecules cGAMP and cCMP/cUMP, respectively, do not include deep positively charged pockets (*16*). Similarly, the internal surfaces of molecule-binding pockets in some members of known sponge families are not substantially positively charged. This was observed, for example, in the structure of the Acb4 sponge from phage SPO1, where the pocket residues in the sponge protein primarily interact with the nucleobases of the signaling molecules (*20*). Different methods should be developed to discover viral sponges and enzymes that do not abide by the biophysical traits common to such proteins.

Most of the proteins that we tested in our screens did not show anti-defense activities against the five defense systems included in this study. Although many of these proteins likely represent false predictions, some of them might be true sponges that bind signaling molecules of defense systems not tested through our assays. The CBASS system that we tested uses 3′3′-cGAMP as its signaling molecule, but other CBASS systems use different molecules, including the cyclic dinucleotides 3′3′-cUA, 3′3′-c-di-UMP, 2′3′-cGAMP, and 3′2′-cGAMP; the cyclic trinucleotides 3′3′3′-cAAG, 3′3′3′-cAAA, and 2′3′3′-cAAA; and more (*5*, *7*–*9*). Some of the nonverified candidate sponges might specifically bind one of these signaling molecules, a possibility that can be explored in future studies. Similarly, proteins in our study might inhibit type III CRISPR-Cas systems that produce cyclic oligo-adenylates as signaling molecules or recently discovered defense systems that rely on inosine derivatives for immune signaling (*40*).

Sponges emerge as a common strategy used by phages to inhibit bacterial immunity. Anti-Thoeris and anti-CBASS sponges were serendipitously detected in five separate unbiased studies aimed to understand how phages inhibit host immunity (*11*, *18*, *19*, *41*, *42*), and our study now further demonstrates the abundance and diversity of sponges in phages. Despite the widespread utilization of sponges by viruses infecting bacteria, it is currently unknown whether viruses infecting eukaryotes use the same counterdefense strategy. Future application of our structure-guided sponge detection approach on the proteomes of animal and plant viruses will enable unbiased searches for sponge proteins in the eukaryotic virus realm.

Materials and methods

Detection of proteins fused to known sponge proteins

The online portal of the Pfam database (*22*) was searched for Pfam protein families that appear fused to either Tad2 (Pfam PF11195) or Acb4 proteins (PF13876). 13 proteins annotated with Pfam PF21825, identified in the IMG/VR4 databased via sequence and structural search as described before (*29*), were taken for further characterization.

Computational pipeline for prediction of positively charged pockets in phage proteome

~32 million phage proteins from ~2 million phage genome scaffolds were clustered based on sequence homology as previously described (*29*), and ~65,000 clusters of short proteins of unknown function with at least 20 members were further analyzed (*29*). To generate multiple sequence alignment for the AlphaFold2 run, the databases of AlphaFold-Multimer 2.3.1 (*31*) with default parameters, with the addition of the IMG/VR v3 database to the default protein databases, were used. AlphaFold-Multimer was then used to predict the structure of a representative sequence (*43*) from each cluster folded as a dimer, trimer, tetramer, pentamer and hexamer, with a single model predicted (model 1) for each homo-oligomer. For predicted structures with a model confidence score (*31*) of at least 0.8, five models were calculated, and structures with an average model confidence score of at least 0.8 over the five models were retained for further analysis. For proteins with more than one possible oligomeric state (score > 0.8), the highest oligomeric form was chosen for further analysis.

Autosite (*33*) and CastP (*32*) with default parameters were ran on each retained homo-oligomeric structure to predict pockets within the structures. Structures in which CastP predicted at least one pocket with a surface area of ≥100 Å^2 and number of corner points ≥150 were further examined, but ignoring pockets with more than 150 atoms. Structures in which Autosite predicted at least one pocket with a score ≥60 were also further examined.

Electrostatic charge spatial maps of the proteins were generated using APBS ver. 3.1.1 (*44*) with the default parameters used in the PyMol APBS plugin. The discrete charge data obtained from the APBS analysis were linearly interpolated to calculate the charge value at the sampled points.

To calculate the surface charge of pockets predicted by the AutoSite software, the Autosite pocket output was first filtered to include only positions ("points") where the distance to the closest atom in the protein was smaller than 1.2 Å. A charge positivity score was computed by calculating the fraction of points that have a charge greater than $5RTe_c^{-1}$ out of the total number of points defining the pocket.

To calculate the surface charge of pockets predicted by CastP, the group of protein atoms that were predicted by CastP to participate in the pocket were analyzed. The solvent accessible surface was defined as the surface encompassing a radius of 1.4 Å around each pocket atom, but excluding areas clashing with other atoms of the protein. Values for the van der Waals radius of atoms were the same values used in PyMOL. The solvent accessible surface was randomly sampled with uniform density of 0.48 Å^{-2}. A charge positivity score was computed by calculating the fraction of the sampled points that have a charge greater than $5RTe_c^{-1}$.

For each protein the pocket with the highest positivity score in the Autosite analysis and the pocket with the highest positivity score in the CastP analysis were further considered. Proteins having at least one pocket with Autosite positivity score of 0.97, or at least one CastP-predicted pocket with positivity score of 0.3, were further examined as possible candidate scores. These thresholds were selected based on a set of 59 predicted structures spanning the structure space of Tad1, Tad2, and Acb2 for which the pockets were characterized previously (*11*, *18*, *19*).

Proteins with pockets that passed the above-mentioned thresholds were searched for homologs in the IMG/VR v3 database using FoldSeek (*25*), and were further examined manually. Candidates whose pockets were not conserved across protein homologs were discarded. Candidates having significant hhpred hit (*e* value ≤ 0.05) to a protein of known function were also discarded. To select candidate proteins for experimental examination, two to eight proteins from each homology group were chosen.

Bacterial strains and growth conditions

E. coli K-12 MG1655 and *Bacillus subtilis* BEST7003 strains were grown in magnesium manganese broth (MMB; LB + 0.1 mM $MnCl_2$ + 5 mM $MgCl_2$) at 37°C shaking at 200 rpm. Whenever applicable, the appropriate antibiotics were added at the following concentrations: For *B. subtilis* strains spectinomycin (100 μg ml^{-1}) and chloramphenicol (5 μg ml^{-1}), and for *E. coli* strains spectinomycin (50 μg ml^{-1}) and kanamycin (50 μg ml^{-1}).

Type I Thoeris from *B. cereus* MSX-D12 (producing 3′cADPR), type II Thoeris from *B. amyloliquefaciens* Y210 (His-ADPR), were cloned previously under their native promoters to the *amyE* locus of the *B. subtilis* BEST7003 genome (*23*). Pycsar from *Bacillus* sp. G1 (cUMP) was cloned similarly under its native promoter to the *amyE* locus.

Type I CBASS from *E. albertii* MOD1-EC1698 (3′3′-cGAMP) (*7*), and Pycsar from *E. coli* E831 (cCMP) (*10*), were integrated into the genome of *E. coli* MG1655 using the Tn7 integration plasmid (spectinomycin resistance, induced by Anhydrotetracycline, Sigma cat. no. 37919) (*45*).

Phage strains

The *B. subtilis* phage SBSphiJ (GenBank: LT960608.1) isolated by us in a previous study was used to perform all infection experiments for type I and type II Thoeris (MOI 0.01, unless stated otherwise). Phi105 (GenBank: NC_048631.1) was obtained from DSMZ (DSM HER46) and was used to infect Pycsar from *Bacillus* sp. G1 (MOI 0.01).

The *E. coli* T2 phage was obtained from DSMZ (16352) and phage Bas60 was obtained from the BASEL phage collection kindly contributed by A. Harms (*28*). Both these phages were used to infect type I CBASS from *E. albertii* (T2 MOI 0.001, Bas60 MOI 10). T5 was kindly contributed by Udi Qimron, and was used to infect Pycsar from *E. coli* E831 (MOI 0.01).

The phages were propagated on either *E. coli* MG1655 or *B. subtilis* BEST7003 by picking a single phage plaque into a liquid culture grown

at 37°C to an optical density at 600 nm (OD_{600}) of 0.3 in MMB broth until culture collapse (or 3 hours in the case of no lysis). The culture was then centrifuged for 10 min at 3200*g* and the supernatant was filtered through a 0.2 μm filter to get rid of remaining bacteria and bacterial debris.

Cloning and transformation of candidate antidefense genes

Candidate antidefense genes were codon optimized for *B. subtilis* and synthesized by Genscript Corp. as pairs under the control of the same isopropyl-ʙ-D-thiogalactopyranoside (IPTG) promoter. Pairs were designed such that candidates showing structural similarity when compared via FoldSeek (*25*) were not placed in the same pair. The sequence "taataaggaggacaaac" was added between the two open reading frames to generate a ribosome binding site. These constructs were subsequently cloned into the thrC-Phspank (*11*) vector, which carries a low-copy pSC101s origin of replication and a kanamycin resistance marker. The resulting plasmid was then introduced into *B. subtilis* BEST7003 cells, where the respective defense system was integrated into the amyE locus, or into *E. coli* K-12 MG1655, where the defense system was integrated downstream of the gmlS gene under the control of an anhydrotetracycline-responsive promoter.

Transformations were performed using a 96-well format. Before transformation, *B. subtilis* BEST7003 cells with or without a defense system were cultured in MC medium at 37°C for 3 hours, as described by Doron *et al.* (*23*). MC medium was composed of 80 mM K2HPO4, 30 mM KH2PO4, 2% glucose, 30 mM trisodium citrate, 22 μg ml^{-1} ferric ammonium citrate, 0.1% casein hydrolysate (CAA) and 0.2% potassium glutamate. Aliquots of 200 μl were transferred to a deep 96-well plate, and 200 ng of the antidefense candidate or control plasmid was added to each well. After a 3 hour incubation at 37°C, 1 ml of MMB medium supplemented with spectinomycin (100 μg ml^{-1}) and chloramphenicol (5 μg ml^{-1}) was added to each well to dilute the MC medium, and the plate was incubated overnight at 30°C. On the following day, a 10 μl aliquot from each well was transferred into 990 μl of fresh MMB containing spectinomycin (100 μg ml^{-1}) and chloramphenicol (5 μg ml^{-1}) for a single passage. After overnight incubation at 37°C, the cultures were used as starters for infection experiments in liquid cultures.

For transformation of *E. coli* K-12 MG1655, cells carrying the defense system integrated into their genome were grown in MMB medium until reaching an OD_{600} of 0.3. The cells were then centrifuged at 3200*g* for 5 min and resuspended in TSS medium at a 20X concentration. A 50 μl aliquot of the cell suspension was distributed into a deep 96-well plate, and 50 ng of the antidefense candidate or control plasmid was added to each well. The transformation protocol consisted of three incubation steps: 5 min on ice, 5 min at room temperature, and an additional 5 min on ice. Subsequently, 500 μl of antibiotic-free MMB was added to each well, followed by incubation with shaking at 37°C for 1 hour. After this recovery period, 500 μl of MMB containing 2x antibiotics: spectinomycin (100 μg ml^{-1}) and kanamycin (100 μg ml^{-1}) was added to each well, to reach a final concentration of 50 μg ml^{-1} spectinomycin and 50 μg ml^{-1} kanamycin, and the plate was incubated overnight at 37°C. On the next day, 10 μl from each well was transferred into 990 μl of fresh MMB containing spectinomycin (50 μg ml^{-1}) and kanamycin (50 μg ml^{-1}) for a single passage. After overnight incubation at 37°C, the cultures were used as starters for infection experiments in liquid cultures.

Infection in liquid culture

Overnight cultures of bacteria harboring the defense system, negative control lacking the system and system + candidate antidefense gene pair were diluted 1:100 in MMB medium. For both *B. subtilis* and *E. coli* cultures, 1 mM IPTG was added to induce expression of candidate antidefense proteins. For *E. coli* cultures anhydrotetracycline (aTC; Sigma cat. no. 37919) was added to induce the expression of the defense system (800 nM and 40 nM for CBASS and Pycsar, respectively). Cells were incubated at 37°C while shaking at 200 rpm until early log phase (OD_{600} of 0.3), and infected in a 96-well plate containing 20 μl of phage lysate. Plates were incubated at 30°C with shaking in a TECAN Infinite200 plate reader and OD_{600} was followed with measurement every 20 min.

Plaque assays

Phage titer was determined using the small drop plaque assay method (*46*). A 300 μl of overnight culture of *E. coli* or *B. subtilis* was mixed with 30 ml MMB 0.5% agar supplemented with 1 mM IPTG (as well as 800 nM and 40 nM of aTC for CBASS and Pycsar, respectively) and poured into a 10-cm square plate followed by incubation for 1 hour at room temperature. Tenfold serial dilutions in MMB were carried out for each of the tested phages and 10 μl drops were put on the bacterial layer. After the drops had dried up, the plates were inverted and incubated overnight at room temperature (for systems expressed in *B. subtilis*) or 37°C (for systems expressed in *E. coli*). PFUs were determined by counting the derived plaques after overnight incubation and lysate titer was determined by calculating PFUs per milliliter. When no individual plaques could be identified, a faint lysis zone across the drop area was considered to be 10 plaques. The efficiency of plating was measured by comparing plaque assay results for control bacteria and those for bacteria containing the defense system and/or the defense system with a candidate antidefense gene.

Preparation of filtered cell lysates for NADase enzymatic assay

For generating filtered cell lysates, *B. subtilis* BEST7003 cells coexpressing the candidate antidefense proteins and the Thoeris system from *B. cereus* MSX-D12 in which ThsA was inactivated (ThsB + ThsAN112A) were used as described previously (*24*). The genes SequestinA, SequestinB, SequestinC, LockinA, and LockinB were integrated in the thrC locus and expressed from an inducible Phspank promoter (*11*). The Thoeris system was integrated in the amyE locus and expressed from its native promoter. Controls included cells expressing only the ThsB + ThsA(N112A) Thoeris system with green fluorescent protein (GFP). All cultures were grown overnight and then diluted 1:100 in 250 ml MMB medium supplemented with 1 mM IPTG and grown at 37°C, 200 rpm shaking for 120 min followed by incubation and shaking at 25°C, 200 rpm until reaching an OD_{600} of 0.3. At this point, a sample of 50 ml was taken as the uninfected sample (time: 0 min), and the SBSphiJ phage was added to the remaining culture at an MOI of 10. Flasks were incubated at 25°C with shaking (200 rpm), for the duration of the experiment. Samples of 50 ml were collected 105 min postinfection. Immediately after sample removal the sample tubes were centrifuged at 4°C for 10 min at 3200*g* to pellet the cells. The supernatant was discarded, and the pellet was flash frozen and stored at −80°C. To extract cell metabolites from frozen pellets, 600 μl of 100 mM Na phosphate buffer (pH 8.0) was added to each pellet. Samples were transferred to FastPrep Lysing Matrix B in a 2 ml tube (MP Biomedicals, cat. no. 116911100) and lysed at 4°C using a FastPrep bead beater for 2 × 40 s at 6 ms^{-1}. Tubes were then centrifuged at 4°C for 10 min at 15,000*g*. The supernatant was then transferred to an Amicon Ultra-0.5 Centrifugal Filter Unit 3 kDa (Merck Millipore, no. UFC500396) and centrifuged for 45 min at 4°C, 12,000*g*. Filtered lysates were taken for in vitro ThsA-based NADase activity assay.

ThsA NADase enzymatic assay

The ThsA protein was expressed and purified as previously described (*18*), and ThsA-based NADase activity assay for the detection of 3′cADPR was carried out as described previously (*24*). NADase reaction was carried out in black 96-well half-area plates (Corning, cat. no. 3694). In each reaction microwell, purified ThsA protein was added to cell lysate, or to 100 mM sodium phosphate buffer pH 8.0. A 5 μl volume of 5 mM nicotinamide 1,N6-ethenoadenine dinucleotide (εNAD^+; Sigma,

cat. no. N2630) solution was added to each well immediately before the beginning of measurements, resulting in a final concentration of 100 nM ThsA protein in a 50 µl final volume reaction. Plates were incubated inside a Tecan Infinite M200 plate reader at 25°C, and measurements were taken at 300 nm excitation wavelength and 410 nm emission wavelength. The reaction rate was calculated from the linear part of the initial reaction.

Preparation of filtered cell lysates for cGAMP measurement

Cells expressing type I CBASS from *E. albertii* MOD1-EC1698 lacking the effector (delta TM) were used, coexpressing the candidate antidefense protein Acb5A, a positive control of Acb2 or a negative control GFP. Cultures were grown overnight and then diluted 1:100 in 200 ml MMB medium supplemented with 1 mM IPTG and 800 nM aTC and grown at 37°C, 200 rpm until reaching an OD_{600} of 0.3. At this point, a sample of 50 ml was taken as the uninfected (time: 0 min) sample, and the Bas60 phage was added to the remaining culture at an MOI of 10. Flasks were incubated at 37°C with shaking (200 rpm), for the duration of the experiment. Samples of 50 ml were collected 30 min postinfection. Immediately after sample removal the sample tubes were centrifuged at 4°C for 10 min at 3200*g* to pellet the cells. The supernatant was discarded, and the pellet was flash frozen and stored at −80°C. To extract cell metabolites from frozen pellets, 600 µl of 100 mM Na phosphate buffer (pH 8.0) was added to each pellet. Samples were transferred to FastPrep Lysing Matrix B in a 2-ml tube (MP Biomedicals, number 116911100) and lysed at 4°C using a FastPrep bead beater for 2 × 40 s at 6 m s^{-1}. Tubes were then centrifuged at 4°C for 10 min at 15,000*g*. The supernatant was then transferred to an Amicon Ultra-0.5 Centrifugal Filter Unit 3 kDa (Merck Millipore, no. UFC500396) and centrifuged for 45 min at 4°C, 12,000*g*. The amount of cGAMP in filtered lysates was measured using a 3′3′-cGAMP enzyme-linked immunosorbent assay (ELISA) kit (Arbor Assays cat. no. K073-H) according to manufacturer's instructions. Limit of detection was calculated during the experiment using a cGAMP standard curve, according to manufacturer's instructions.

Synthesis of radiolabeled cyclic nucleotide signals

Cyclic nucleotides were synthesized using the following purified recombinant enzymes: *Vibrio cholerae* DncV (*9*): 3′3′-c-di-AMP, 3′3′-cGAMP, and 3′3′-c-di-GMP; and *Yersinia aleksiciae* CdnE: 3′3′-cUA (*7*). Cyclic nucleotide synthesis was performed at 37°C for ~20 hours in 10 µl reactions containing a final concentration of 5 µM recombinant enzyme, 20 µM appropriate nucleotide triphosphates (NTPs), trace amounts of appropriate α-^{32}P–labeled NTP (Revvity), 25 mM KCl, 5 mM $MgCl_2$, 1 mM $MnCl_2$, 1 mM TCEP and 50 mM Tris-HCl pH 7.5 (DncV) or pH 9.0 (*Ya*CdnE). After overnight incubation, reactions were centrifuged at 17,000*g* for 1 min to remove any precipitated protein. To digest unincorporated NTPs, clarified synthesis reactions were treated with 2 µl of Quick CIP (NEB) followed by incubation for ~30 min at 37°C and heat inactivation for 2 min at 80°C. To confirm cyclic nucleotide synthesis, ~1 µl of the final reaction product was spotted on a PEI cellulose TLC plate (Sigma Aldrich) and developed in a 1.5 M KH_2PO_4 (pH 3.8) buffer for 90 min. Plates were dried at room temperature for ~20 min, exposed to a storage phosphor screen, and imaged with a Typhoon Trio Variable Mode Imager System (GE Healthcare).

Analysis of cyclic nucleotide degradation by TLC

TLC was used to analyze Acb5A cyclic nucleotide degradation. Degradation reactions were performed at 37°C in 5 µl reactions containing 5 µM recombinant Acb5, 5 µM of α-^{32}P–labeled cyclic dinucleotide, 50 mM Tris-HCl pH 7.5, 5 mM $MgCl_2$, 10 mM KCl, and 1 mM TCEP. After 30 min incubation, reactions were boiled at 95°C for 3 min and centrifuged at 17,000*g* for 1 min. 1 µl of the boiled reaction was spotted on a 20 cm × 20 cm PEI cellulose TLC plate (Sigma Aldrich) and developed in a 1.5 M KH_2PO_4 (pH 3.8) buffer for 90 min. Plates were dried at room temperature for ~20 min, exposed to a storage phosphor screen, and imaged with a Typhoon Trio Variable Mode Imager System (GE Healthcare).

Lockin–3′cADPR crystallization and structure determination

Crystals of the Lockin–3′cADPR complex were grown using hanging-drop vapor diffusion method for ~12 days at 18°C. Recombinant Lockin was diluted to 10 mg ml^{-1} in a buffer containing 20 mM Tris-HCl pH 7.5, 250 mM KCl, and 1 mM TCEP. The diluted protein was incubated with 500 µM 3′cADPR (Biolog Life Science Institute) on ice for ~30 min. The resultant protein mixture was allowed to equilibrate to 18°C and crystals were grown in 96-well trays containing 70 µl reservoir solution and 800 nl drops. Drops were mixed 1:1 with purified protein and reservoir solution (11.5% PEG-6000, 0.1 M HEPES pH 7.5, and 5% (*v*/*v*) MPD). Crystals were cryo-protected with reservoir solution supplemented with 20% (*v*/*v*) glycerol and 500 µM 3′cADPR (Biolog Life Science Institute) and harvested by flash-freezing in liquid nitrogen. X-ray diffraction data were collected at Advanced Photon Source (beamline 24-ID-E), and data were processed on the RAPDv2 platform using XDS (*47*). Experimental phase information was determined by molecular replacement using Phaser-MR in PHENIX (*48*) and a model of Lockin generated using AlphaFold3 (*49*). Model building was performed using Coot (*50*) and refined using PHENIX. A summary of crystallographic statistics is provided in table S7. All structural figures were generated using PyMOL (Version 2.5.4, Schrödinger, LLC).

Protein expression and purification

The antidefense genes were cloned (TWIST Bioscience, USA) into the expression vector pET28-His-bdSumo. pET28-His-bdSumo was constructed by transferring the His14-bdSUMO cassette from the K151 expression vector generously donated by D. Görlich from the Max-Planck-Institute, Göttingen, Germany (*51*) into the expression vector pET28-TevH (*52*).

Each protein was expressed in *E. coli* LOBSTR-BL21(DE3)-RIL (Kerafast, USA) by induction with 500 µM IPTG at 16°C overnight. The culture was harvested and lysed on ice by a EmulsiFlex-C3 (Avestin, Canada) in a lysis buffer [20 mM HEPES pH 7.3, 0.4 M NaCl, 1 mM dithiothreitol (DTT), 30 mM imidazole]. After centrifugation (20,000*g*, 30 min, 4°C), the supernatant was filtered through a 0.4 µm filter, and sample was loaded on a HisTrap FF 5 ml column (Cytiva) prewashed with lysis-buffer. The column was subsequently washed with lysis-buffer followed by a wash buffer containing high salt (20 mM HEPES pH 7.3, 1 M NaCl, 1 mM DTT, 30 mM imidazole). The protein was eluted using elution buffer (buffer 20 mM HEPES pH 7.3, 0.4 M NaCl, 1 mM DTT, 300 mM imidazole), and was inserted into a 3.5 MWCO 15 ml slide-A lyzer (Thermoscientific) with 0.4 mg of His-bdSENP1 protease to cleave the target protein from its His-bdSUMO tag and dialyzed against cleavage buffer (20 mM HEPES, 125 mM KCl, 1 mM DTT) overnight at 4°C. The sample was centrifuged again (20,000*g*, 30 min, 4°C), filtered, supplemented with NaCl and imidazole to final conc. of 275 mM NaCl and 40 mM imidazole. The sample was then reapplied to a HisTrap FF 5 ml column (Cytiva) to recapture the His-bdSUMO tag uncleaved precursor and the His-tagged bdSENP1 protease. Flowthrough containing the cleaved antidefense protein was then passed through an Amicon ULTR-15 30 MWCO filter, to remove any remaining residual cleaved His-SUMO tag and His-tagged bdSENP1 protease. The protein was then stored at −80°C.

Mass photometry

Mass photometry (*53*) measurements were acquired using a OneMP mass photometer (Refeyn Ltd). Microscope coverslips (no. 1.5, 24 × 50 Marienfeld, 0107222) were cleaned by sequential sonication in 50% isopropanol (HPLC grade) in Milli-Q H2O, and Milli-Q H2O (5 min each), followed by drying with a clean nitrogen stream. Four reusable culture-well gaskets 3 mm diameter × 1 mm depth (Sigma, GBL103250-10EA) were cut, washed with ethanol followed by MilliQ water and

dried using nitrogen stream. Dried gaskets were placed at the center of the coverslip, where each well was used for one measurement. To establish focus, fresh 100 mM sodium phosphate (pH 8) buffer (15 µl) was first loaded into the well, the focal position was identified and secured in place for the entire measurement, with an autofocus system based on total internal reflection. Molecular weights were calibrated using pure bovine serum albumin (BSA) and bovine immunoglobulin Gs (IgGs) standards.

Purified LockinA and SequestinA proteins were diluted to a concentration of 10 nM or 50 nM, respectively. For each measurement, 5 µl of protein was introduced into the measurement well with the loaded buffer and mixed several times. After autofocus stabilization, movies were recorded for a duration of 120 s. Data acquisition was performed using AcquireMP (Refeyn Ltd, v.2.3) and data analysis was performed using DiscoverMP (Refeyn Ltd, v.2.3).

Knock-in of Sequestin and Lockin candidates into phage SBSphiJ

The DNA sequence of the genes was amplified from the respective pSG-thrC-Phspank plasmid, or in the case of T4-Y16Q from the phage genome itself, using KAPA HiFi HotStart ReadyMix (Roche, cat. no. KK2601) with the following primer pairs:

LockinA: ttttatacctataggaggtagctATGAAAGAAAAAGATCTTGGAATCACTGA, ttttccctccagttgttcTTAAATTTTTCCGATAAAACGAGTGTTGC.

LockinB: ttttatacctataggaggtagctATGACCGTGGAGAAAACATTGAC, ttttccctccagttgttcTCACGGATCGATAAGATCTACGTAGC.

LockinC: ttttatacctataggaggtagctATGAACATGGACAAAAAGGAAGAGAA, ttttccctccagttgttcTTACGGGCGTGTGATTGAATATGTG.

SequestinA: tcaaattttatacctataggaggtagctatgGAGAAGTCTGTTTTTTGATCGCCTGC, tttgccaagtgttttccctccagttgttcttaTTCATTAATCGTAGATTTCGCCAACGC.

SequestinB: tcaaattttatacctataggaggtagctatgCAAGACTTTCAACAGCGGGTA, tttgccaagtgttttccctccagttgttcttaGATCTCAAAGCCCGCAATGCG.

T4-Y16Q: tcaaattttatacctataggaggtagctatgttagcttatcaagcacgagtaaaag, tttgccaagtgttttccctccagttgttcttacttgaattgtgcaattcttttctctagac.

The backbone fragment with the upstream and downstream genomic arms (±1.2 kb) for the integration site of candidate was amplified from the plasmid used previously for knock-in of the *tad1* gene (*11*) (F-gaacaactggagggaaaacacttg, R-agctacctcctataggtataaaatttg). Cloning was carried out using the NEBuilder HiFi DNA Assembly cloning kit *(NEB, cat. no. E5520S) and the cloned vector was transformed into* NEB 5-alpha competent cells. The cloned vector was subsequently transformed into the thrC site of *B. subtilis* BEST7003. To amplify phages, the antidefense-containing *B. subtilis* BEST7003 strain was infected with phage SBSphiJ with an MOI of 0.1 and cell lysate was collected. Phages with knock-in were selected by Cas13a-gRNA-SBSphiJ strain (*54*). The selection was made on an agar plate in the presence of 0.2% xylose to induce Cas13. Resistant phages were purified three times on *B. subtilis* BEST7003. Purified phages were verified again for the presence of the antidefense candidate using polymerase chain reaction (PCR) and sequencing.

Distribution of antidefense proteins in phage genomes

Homologs of verified antidefense genes were identified in the IMG/VR v4 database by conducting sequence-based and structure-based homology searches as described previously (*29*). For this, 5.5 million phage scaffolds labeled as "high-confidence virus" were downloaded from the IMG/VR v4 database. Homologous sequences of the antidefense proteins detected in this study were identified using the "search" option of MMseqs2 release 13-45111 with the parameters "-c 0.8 –cov-mode 2." To identify structural homologs, the downloaded proteins from IMG/VR v4 were clustered using the "cluster" option of MMseqs2 with default parameters. Next, a representative sequence was extracted from each cluster containing at least 30 nonidentical members, and its structure was predicted using AlphaFold2 version 2.3 with default parameters, resulting in 182,179 phage protein structures. Structures of the antidefense proteins were searched against this set of 182,179 phage protein structures using Foldseek release 5.53465f065 with default parameters. Hits with probability of 1.0 and no additional protein domains outside of the homology region were collected with all their cluster members as structural homologs of the antidefense proteins. Protein members belonging to clusters containing an additional domain outside of the homology region were defined as homologs if they also had any significant sequence similarity to the verified antidefense proteins, using the "search" option of MMseqs2 with default parameters. Homologs of antidefense proteins were detected in the INPHARED database and in the BASEL phage collection using the "search" option of MMseqs2 with the parameter "-c 0.8," using all of the antidefense homologs detected in IMG/VR v4 as queries.

SequestinA and LockinA in vitro sponge experiment

SequestinA and LockinA were expressed and purified as described above in the protein expression and purification section. Sponge and ligand (3′cADPR, Biolog cat. no. C 404) were mixed in a 1:1 ratio to a final concentration of 100 uM, in 100 mM sodium phosphate buffer pH 8.0. Ligand and sponge, as well as a control containing the ligand only, were incubated for 10 min at room temperature. After the incubation the samples were filtered through a 3 kDa MWCO filter, and flow through was collected and analyzed by HPLC. The upper fractions (containing the protein + ligand complexes) were washed by successive concentration and dilution in a 3 kDa MWCO filter with five 1:20 dilutions in phosphate-buffered saline (PBS). For LockinA the upper fraction was then boiled at 98°C for 10 min, pelleted at 13,500*g* for 20 min, and filtered through a 3 kDa MWCO filter. The filtrate was collected and assessed by HPLC. For SequestinA, the upper fraction was then subjected to chloroform denaturation as follows. 200 µl of the sample were mixed with 200 µl of phenol:chloroform:isoamyl alcohol (25:24:1), vortexed for 1 min and centrifuged at 10,000*g* for 10 min. The aquatic phase was taken and mixed with 200 µl chloroform:Isoamyl alcohol (24:1), vortexed for 1 min, centrifuged at 10,000*g* for 10 min and 10 µl of the aquatic phase was taken and analyzed by HPLC.

Acb5A enzymatic reaction

Acb5A enzymatic reaction was carried out by mixing a purified Acb5A with its ligand (3′3′-cGAMP, Biolog cat. no. C117) in a 1:100 ratio (1 µM Acb5A, 100 µM 3′3′-cGAMP) in 0.1 M phosphate buffer (sodium phosphate pH8). 200 µl were collected at each time point. Time point 0′ was taken before adding the enzyme, and time point 30′ was taken after 30 min of incubation at 30°C. Similarly, Acb5A was mixed with cUA (Biolog cat. no. C357) in a ratio of 1:100 (1 µM Acb5A, 100 µM cUA) in 0.1M phosphate buffer. Time point 0′ was taken before adding the enzyme, and time point 60′ was taken after 60 min of incubation at 30°C. After incubation, the samples were filtered through a 3 kDa MWCO filter, and flow through was collected and analyzed by HPLC.

HPLC analysis

10 µl of the samples were analyzed using HPLC. HPLC of the obtained fraction was performed using Agilent 1260 and chromatography SUPELCOSIL LC-18-T HPLC Column. The following protocol was used for all runs: 1 min of mobile phase A 100%, 2 min 75% A and 25% B, 2 min 50% A and 50% B, 2 min 20% A and 80% B and 3 min 100% A, 1 ml/min flow rate. Mobile phase A was 20 mM potassium phosphate pH 6 and B was 20 mM potassium phosphate pH 6 in 20% methanol.

Liquid chromatography–mass spectrometry (LC-MS) polar metabolite analysis

The sample collected for HPLC were also analyzed by UPLC–high-resolution mass spectrometry (HRMS) without dilution. The analyses were carried out on a Waters SYNAPT-XS Q-Tof mass spectrometer (Manchester, UK) with an electrospray ionization (ESI) source. The spectra cGAMP, cGMP, cAMP and cUA were recorded in the negative

ion mode within a mass range from 100 to 1200 m/z. The parameters were set as follows: capillary voltage at 1.5 kV, cone gas flow at 50 l/h, source temperature at 140°C, and cone voltage at 20 V. The desolvation temperature was set at 600°C, and the desolvation gas (N_2) flow rate was set at 800 l/h. Lock spray was acquired with Leucine Encephalin (m/z = 554.2615 in negative mode) at a concentration of 200 ng/ml and a flow rate of 10 µl/min once every 10 s for 1 s period to ensure mass accuracy. Waters MassLynx v4.2 software was used for data acquisition and data processing. The analytes were separated using Waters Premier Acquity UPLC system. The gradient elution was achieved with Waters Acquity Premier HSS T3 Column, 1.8 µm, 2.1 × 100 mm at 0.25 ml/min flow rate, 35°C. Mobile phase A consisted of 0.1% of aqueous formic acid (Fisher Scientific A117-50) and mobile phase B consisted of 0.1% formic acid in acetonitrile:water (95:5). Identification of substrates and products was done by MS and retention time, and validated by the injection of a commercially available standard.

Analytical SEC analysis of apo and ligand-bound SequestinA and LockinA

17.2 µl volume of LockinA (218 µM) or 15 µl of SequestinA (250 µM) protein was incubated with 7.5 µl of 3′cADPR (5 mM) and mixed with PBS buffer (final volume of 100 µl) at 25°C for 10 min. As a control, the apo protein was incubated under identical conditions without the ligand. After incubation, each sample was loaded onto a Superdex 200 Increase 10/300 GL (Cytiva) SEC column, pre-equilibrated with PBS buffer. Chromatography was performed at a flow rate of 0.6 ml/min at 4°C using an ÄKTA purifier, and sample was monitored by absorbance at both 260 nm and 280 nm.

Protein mass spectrometry

E. coli strains expressing Acb5, along with an RFP control strains, were diluted 1:100 from overnight cultures into fresh medium supplemented with 1 mM IPTG. Similarly, *B. subtilis* strains expressing Sequestin or Lockin, as well as a GFP control strains, were diluted 1:25 from overnight cultures in medium containing 1 mM IPTG. Cultures were grown until reaching an OD_{600} of 0.6, after which cells were harvested by centrifugation at 3900*g* for 10 min. Cell pellets were resuspended in 2 ml PBS and centrifuged again at 13,000*g* for 10 min. The resulting pellets were flash-frozen in a dry ice–ethanol bath and stored at −80°C. Cell pellets were then lysed with 5% SDS in 50 mM Tris-HCl. Lysates were incubated at 96°C for 5 min, followed by 10 cycles of 30 s of sonication (Bioruptor Pico, Diagenode, USA). Protein concentration was measured using the BCA assay (Thermo Scientific, USA) and a total of 50 µg protein was reduced with 5 mM dithiothreitol and alkylated with 10 mM iodoacetamide in the dark. Phosphoric acid was added to the lysates to a final concentration of 1.2%, followed by the addition of 90% methanol in 5 mM ammonium bicarbonate. Each sample was then loaded onto an S-Trap 96-well plate (Protifi, USA). Samples were then digested with trypsin (1:50 trypsin/protein) O/N h at 37°C. The digested peptides were eluted using 50 mM ammonium bicarbonate; trypsin was added to this fraction and incubated 4 hours at 37°C. Two more elutions were made using 0.2% formic acid and 0.2% formic acid in 50% acetonitrile. The three elutions were pooled together and vacuum-centrifuged to dry. Samples were kept at −20°C until analysis.

ULC/MS grade solvents were used for all chromatographic steps. Each sample was loaded using split-less nano-Ultra Performance Liquid Chromatography (10 kpsi Acquity M-Class; Waters, Milford, MA, USA). The mobile phase was: A) H2O + 0.1% formic acid and B) acetonitrile + 0.1% formic acid. Desalting of the samples was performed online using a reversed-phase Symmetry C18 trapping column (180 µm internal diameter, 20 mm length, 5 µm particle size; Waters). The peptides were then separated using a T3 HSS nano-column (75 µm internal diameter, 250 mm length, 1.8 µm particle size; Waters) at 0.35 µl/min. Peptides were eluted from the column into the mass spectrometer using the following gradient: 4% to 30% B in 105 min, 30% to 90% B in 10 min, maintained at 90% for 7 min and then back to initial conditions.

The nanoUPLC was coupled online through a nanoESI emitter (10 µm tip; New Objective; Woburn, MA, USA) to a quadrupole orbitrap mass spectrometer (Exploris 480, Thermo Scientific) using a FlexIon nanospray apparatus (Proxeon). Data were acquired in data-dependent acquisition (DDA) mode. MS1 resolution was set to 120,000 (at 400 m/z), mass range of 380 to 1500 m/z, 200% AGC and maximum injection time was set to 50 ms. MS2 resolution was set to 15,000, quadrupole isolation 1.4 m/z, 75% AGC, dynamic exclusion of 40 s and Auto maximum injection time. A preferential inclusion list was specified for higher priority of MS/MS triggering. The list of peptides is provided as table S1.

Raw data were processed using Proteome Discoverer v2.4.1.15. MS/MS spectra were searched using Sequest HT. Data were searched against the *E. coli* or *B. subtilis* sequences UniprotKB (https://www.uniprot.org/) appended with common laboratory contaminant proteins and the mutated sequences. Fixed modification was set to carbamidomethylation of cysteines and variable modification was set to oxidation of methionines and acetylation, methionine loss and their combination at protein N termini. Proteins were filtered to global false discovery rate of maximum of 1% using the percolator node.

Prediction of protein-ligand contacts

AlphaFold3 (*49*) was used to generate structural models for all sponges or enzymes with their ligands. RING 4.0 (*55*) was applied to identify possible ligand-interacting residues together with manual examination for evolutionary conserved residues adjacent to the ligand.

REFERENCES AND NOTES

1. S. J. Hobbs, P. J. Kranzusch, Nucleotide Immune Signaling in CBASS, Pycsar, Thoeris, and CRISPR Antiphage Defense. *Annu. Rev. Microbiol.* **78**, 255–276 (2024). doi: 10.1146/annurev-micro-041222-024843; pmid: 39083849
2. S. Dvorkin, S. Cambier, H. E. Volkman, D. B. Stetson, New frontiers in the cGAS-STING intracellular DNA-sensing pathway. *Immunity* **57**, 718–730 (2024). doi: 10.1016/j.immuni.2024.02.019; pmid: 38599167
3. D. Lapin, O. Johanndrees, Z. Wu, X. Li, J. E. Parker, Molecular innovations in plant TIR-based immunity signaling. *Plant Cell* **34**, 1479–1496 (2022). doi: 10.1093/plcell/koac035; pmid: 35143666
4. L. Sun, J. Wu, F. Du, X. Chen, Z. J. Chen, Cyclic GMP-AMP synthase is a cytosolic DNA sensor that activates the type I interferon pathway. *Science* **339**, 786–791 (2013). doi: 10.1126/science.1232458; pmid: 23258413
5. D. Cohen *et al.*, Cyclic GMP-AMP signalling protects bacteria against viral infection. *Nature* **574**, 691–695 (2019). doi: 10.1038/s41586-019-1605-5; pmid: 31533127
6. B. R. Morehouse *et al.*, STING cyclic dinucleotide sensing originated in bacteria. *Nature* **586**, 429–433 (2020). doi: 10.1038/s41586-020-2719-5; pmid: 32877915
7. B. Duncan-Lowey, N. K. McNamara-Bordewick, N. Tal, R. Sorek, P. J. Kranzusch, Effector-mediated membrane disruption controls cell death in CBASS antiphage defense. *Mol. Cell* **81**, 5039–5051.e5 (2021). doi: 10.1016/j.molcel.2021.10.020; pmid: 34784509
8. A. Millman, S. Melamed, G. Amitai, R. Sorek, Diversity and classification of cyclic-oligonucleotide-based anti-phage signalling systems. *Nat. Microbiol.* **5**, 1608–1615 (2020). doi: 10.1038/s41564-020-0777-y; pmid: 32839535
9. A. T. Whiteley *et al.*, Bacterial cGAS-like enzymes synthesize diverse nucleotide signals. *Nature* **567**, 194–199 (2019). doi: 10.1038/s41586-019-0953-5; pmid: 30787435
10. N. Tal *et al.*, Cyclic CMP and cyclic UMP mediate bacterial immunity against phages. *Cell* **184**, 5728–5739.e16 (2021). doi: 10.1016/j.cell.2021.09.031; pmid: 34644530
11. A. Leavitt *et al.*, Viruses inhibit TIR gcADPR signalling to overcome bacterial defence. *Nature* **611**, 326–331 (2022). doi: 10.1038/s41586-022-05375-9; pmid: 36174646
12. D. Sabonis *et al.*, TIR domains produce histidine-ADPR as an immune signal in bacteria. *Nature* **642**, 467–473 (2025). doi: 10.1038/s41586-025-08930-2; pmid: 40307559
13. F. Rousset *et al.*, TIR signaling activates caspase-like immunity in bacteria. *Science* **387**, 510–516 (2025). doi: 10.1126/science.adu2262; pmid: 39883761
14. T. Wein, R. Sorek, Bacterial origins of human cell-autonomous innate immune mechanisms. *Nat. Rev. Immunol.* **22**, 629–638 (2022). doi: 10.1038/s41577-022-00705-4; pmid: 35396464
15. D. Mayo-Muñoz, R. Pinilla-Redondo, S. Camara-Wilpert, N. Birkholz, P. C. Fineran, Inhibitors of bacterial immune systems: Discovery, mechanisms and applications. *Nat. Rev. Genet.* **25**, 237–254 (2024). doi: 10.1038/s41576-023-00676-9; pmid: 38291236

16. S. J. Hobbs *et al.*, Phage anti-CBASS and anti-Pycsar nucleases subvert bacterial immunity. *Nature* **605**, 522–526 (2022). doi: 10.1038/s41586-022-04716-y; pmid: 35395152
17. J. B. Eaglesham, Y. Pan, T. S. Kupper, P. J. Kranzusch, Viral and metazoan poxins are cGAMP-specific nucleases that restrict cGAS–STING signalling. *Nature* **566**, 259–263 (2019). doi: 10.1038/s41586-019-0928-6; pmid: 30728498
18. E. Yirmiya *et al.*, Phages overcome bacterial immunity via diverse anti-defence proteins. *Nature* **625**, 352–359 (2024). doi: 10.1038/s41586-023-06869-w; pmid: 37992756
19. E. Huiting *et al.*, Bacteriophages inhibit and evade cGAS-like immune function in bacteria. *Cell* **186**, 864–876.e21 (2023). doi: 10.1016/j.cell.2022.12.041; pmid: 36750095
20. R. B. Chang *et al.*, A widespread family of viral sponge proteins reveals specific inhibition of nucleotide signals in anti-phage defense. *Mol. Cell* **85**, 3151–3165.e6 (2025). doi: 10.1016/j.molcel.2025.07.016
21. D. Li *et al.*, Single phage proteins sequester signals from TIR and cGAS-like enzymes. *Nature* **635**, 719–727 (2024). doi: 10.1038/s41586-024-08122-4; pmid: 39478223
22. J. Mistry *et al.*, Pfam: The protein families database in 2021. *Nucleic Acids Res.* **49**, D412–D419 (2021). doi: 10.1093/nar/gkaa913; pmid: 33125078
23. S. Doron *et al.*, Systematic discovery of antiphage defense systems in the microbial pangenome. *Science* **359**, eaar4120 (2018). doi: 10.1126/science.aar4120; pmid: 29371424
24. G. Ofir *et al.*, Antiviral activity of bacterial TIR domains via immune signalling molecules. *Nature* **600**, 116–120 (2021). doi: 10.1038/s41586-021-04098-7; pmid: 34853457
25. M. van Kempen *et al.*, Fast and accurate protein structure search with Foldseek. *Nat. Biotechnol.* **42**, 243–246 (2024). doi: 10.1038/s41587-023-01773-0; pmid: 37156916
26. A. P. Camargo *et al.*, IMG/VR v4: An expanded database of uncultivated virus genomes within a framework of extensive functional, taxonomic, and ecological metadata. *Nucleic Acids Res.* **51**, D733–D743 (2023). doi: 10.1093/nar/gkac1037; pmid: 36399502
27. R. Cook *et al.*, INfrastructure for a PHAge REference Database: Identification of Large-Scale Biases in the Current Collection of Cultured Phage Genomes. *Phage* **2**, 214–223 (2021). doi: 10.1089/phage.2021.0007; pmid: 36159887
28. E. Maffei *et al.*, Systematic exploration of *Escherichia coli* phage–host interactions with the BASEL phage collection. *PLOS Biol.* **19**, e3001424 (2021). doi: 10.1371/journal.pbio.3001424; pmid: 34784345
29. E. Yirmiya *et al.*, Structure-guided discovery of viral proteins that inhibit host immunity. *Cell* **188**, 1681–1692.e17 (2025). doi: 10.1016/j.cell.2024.12.035; pmid: 39855193
30. S. Roux *et al.*, IMG/VR v3: An integrated ecological and evolutionary framework for interrogating genomes of uncultivated viruses. *Nucleic Acids Res.* **49**, D764–D775 (2021). doi: 10.1093/nar/gkaa946; pmid: 33137183
31. R. Evans *et al.*, Protein complex prediction with AlphaFold-Multimer. bioRxiv 2021.10.04.463034 [Preprint] (2022). doi: 10.1101/2021.10.04.463034
32. T. A. Binkowski, S. Naghibzadeh, J. Liang, CASTp: Computed Atlas of Surface Topography of proteins. *Nucleic Acids Res.* **31**, 3352–3355 (2003). doi: 10.1093/nar/gkg512; pmid: 12824325
33. P. A. Ravindranath, M. F. Sanner, AutoSite: An automated approach for pseudo-ligands prediction—from ligand-binding sites identification to predicting key ligand atoms. *Bioinformatics* **32**, 3142–3149 (2016). doi: 10.1093/bioinformatics/btw367; pmid: 27354702
34. D. delToro *et al.*, Walker-A Motif Acts to Coordinate ATP Hydrolysis with Motor |Output in Viral DNA Packaging. *J. Mol. Biol.* **428**, 2709–2729 (2016). doi: 10.1016/j.jmb.2016.04.029; pmid: 27139643
35. L. M. Longo *et al.*, On the emergence of P-Loop NTPase and Rossmann enzymes from a Beta-Alpha-Beta ancestral fragment. *eLife* **9**, e64415 (2020). doi: 10.7554/eLife.64415; pmid: 33295875
36. R. D. Requião *et al.*, Viruses with different genome types adopt a similar strategy to pack nucleic acids based on positively charged protein domains. *Sci. Rep.* **10**, 5470 (2020). doi: 10.1038/s41598-020-62328-w; pmid: 32214181
37. J. D. Perlmutter, M. F. Hagan, Mechanisms of virus assembly. *Annu. Rev. Phys. Chem.* **66**, 217–239 (2015). doi: 10.1146/annurev-physchem-040214-121637; pmid: 25532951
38. J. S. Athukoralage *et al.*, An anti-CRISPR viral ring nuclease subverts type III CRISPR immunity. *Nature* **577**, 572–575 (2020). doi: 10.1038/s41586-019-1909-5; pmid: 31942067
39. S. J. Hobbs, J. Nomburg, J. A. Doudna, P. J. Kranzusch, Animal and bacterial viruses share conserved mechanisms of immune evasion. *Cell* **187**, 5530–5539.e8 (2024). doi: 10.1016/j.cell.2024.07.057; pmid: 39197447
40. Z. Zeng *et al.*, Base-modified nucleotides mediate immune signaling in bacteria. *Science* **388**, eads6055 (2025). doi: 10.1126/science.ads6055; pmid: 39977546
41. X. Cao *et al.*, Phage anti-CBASS protein simultaneously sequesters cyclic trinucleotides and dinucleotides. *Mol. Cell* **84**, 375–385.e7 (2024). doi: 10.1016/j.molcel.2023.11.026; pmid: 38103556
42. J. M. Jenson, T. Li, F. Du, C.-K. Ea, Z. J. Chen, Ubiquitin-like conjugation by bacterial cGAS enhances anti-phage defence. *Nature* **616**, 326–331 (2023). doi: 10.1038/s41586-023-05862-7; pmid: 36848932
43. M. Steinegger, J. Söding, MMseqs2 enables sensitive protein sequence searching for the analysis of massive data sets. *Nat. Biotechnol.* **35**, 1026–1028 (2017). doi: 10.1038/nbt.3988; pmid: 29035372
44. N. A. Baker, D. Sept, S. Joseph, M. J. Holst, J. A. McCammon, Electrostatics of nanosystems: Application to microtubules and the ribosome. *Proc. Natl. Acad. Sci. U.S.A.* **98**, 10037–10041 (2001). doi: 10.1073/pnas.181342398; pmid: 11517324
45. W. Jasinska *et al.*, Chromosomal barcoding of *E. coli* populations reveals lineage diversity dynamics at high resolution. *Nat. Ecol. Evol.* **4**, 437–452 (2020). doi: 10.1038/s41559-020-1103-z; pmid: 32094541
46. A. Mazzocco, T. E. Waddell, E. Lingohr, R. P. Johnson, in *Bacteriophages: Methods and Protocols, Volume 1: Isolation, Characterization, and Interactions*, M. R. J. Clokie, A. M. Kropinski, Eds., **vol. 501** of *Methods in Molecular Biology* (Humana Press, 2009), pp. 81–85.doi: 10.1007/978-1-60327-164-6_9
47. W. Kabsch, XDS. *Acta Crystallogr. D* **66**, 125–132 (2010). doi: 10.1107/S0907444909047337; pmid: 20124692
48. D. Liebschner *et al.*, Macromolecular structure determination using X-rays, neutrons and electrons: Recent developments in *Phenix*. *Acta Crystallogr. D* **75**, 861–877 (2019). doi: 10.1107/S2059798319011471; pmid: 31588918
49. J. Abramson *et al.*, Accurate structure prediction of biomolecular interactions with AlphaFold 3. *Nature* **630**, 493–500 (2024). doi: 10.1038/s41586-024-07487-w; pmid: 38718835
50. P. Emsley, B. Lohkamp, W. G. Scott, K. Cowtan, Features and development of *Coot*. *Acta Crystallogr. D* **66**, 486–501 (2010). doi: 10.1107/S0907444910007493; pmid: 20383002
51. S. Frey, D. Görlich, A new set of highly efficient, tag-cleaving proteases for purifying recombinant proteins. *J. Chromatogr. A* **1337**, 95–105 (2014). doi: 10.1016/j.chroma.2014.02.029; pmid: 24636565
52. Y. Peleg, T. Unger, Application of high-throughput methodologies to the expression of recombinant proteins in *E. coli*. *Methods Mol. Biol.* **426**, 197–208 (2008). doi: 10.1007/978-1-60327-058-8_12; pmid: 18542865
53. A. Sonn-Segev *et al.*, Quantifying the heterogeneity of macromolecular machines by mass photometry. *Nat. Commun.* **11**, 1772 (2020). doi: 10.1038/s41467-020-15642-w; pmid: 32286308
54. I. Osterman *et al.*, Phages reconstitute NAD^+ to counter bacterial immunity. *Nature* **634**, 1160–1167 (2024). doi: 10.1038/s41586-024-07986-w; pmid: 39322677
55. A. Del Conte *et al.*, RING 4.0: Faster residue interaction networks with novel interaction types across over 35,000 different chemical structures. *Nucleic Acids Res.* **52**, W306–W312 (2024). doi: 10.1093/nar/gkae337; pmid: 38686797

ACKNOWLEDGMENTS

We thank members of the Sorek and Kranzusch laboratory for constructive discussion during this study, Y. Peleg and S. Albeck for assistance with protein expression, and M. Kupervaser and A. Savidor for assistance with protein mass spectrometry. **Funding:** R.S. was supported, in part, by the European Research Council (grant ERC-AdG GA 101018520), the Israel Science Foundation (MAPATS grant 2720/22), the Minerva Foundation with funding from the Federal German Ministry for Education and Research, a research grant from the Estate of Hermine Miller, the Institute for Environmental Sustainability (IES) and the Center for Immunotherapy at the Weizmann Institute of Science, and the Knell Family Center for Microbiology. The research was supported in part by grants to P.J.K. from the Burroughs Wellcome Fund PATH program, The G. Harold and Leila Y. Mathers Charitable Foundation, the Cancer Research Institute, the Parker Institute for Cancer Immunotherapy, the Massachusetts Consortium on Pathogen Readiness (MassCPR), the Gates Foundation (INV-083469), and the National Institutes of Health (1DP2GM146250-01). E.Y. was supported by the Clore Scholars Program and, in part, by the Israeli Council for Higher Education (CHE) through the Weizmann Data Science Research Center. R.B.C. is supported through a Landry Cancer Biology Research Fellowship (Harvard Faculty of Arts and Sciences). X-ray data were collected at the Northeastern Collaborative Access Team beamlines, which are funded by the National Institute of General Medical Sciences from the National Institutes of Health (P30 GM124165). The Eiger 16M detector on the 24-ID-E beamline is funded by a NIH-ORIP HEI grant (S10OD021527). This research used resources of the Advanced Photon Source, a US Department of Energy (DOE) Office of Science User Facility operated for the DOE Office of Science by Argonne National Laboratory under contract no. DE-AC02-06CH11357. This publication resulted from the data collected using the beamtime obtained through NECAT BAG proposal no. 311950. **Author contributions:** Conceptualization: R.S., N.T.; Funding acquisition: R.S., P.J.K., R.B.C., E.Y.; Investigation: N.T., R.H., R.B.C., I.O., R.J., E.Y., N.B., D.H., M.L.R., B.M., M.G., T.W., G.A.; Methodology: R.S., N.T., R.H., J.G., I.O., G.A., R.J., R.B.C.; Project administration: R.S., N.T.; Supervision: R.S., P.J.K.; Visualization: N.T.; Writing – original draft: R.S., N.T., P.J.K.; Writing – review & editing: R.S., N.T. **Competing interests:** R.S. is a scientific cofounder and adviser of BiomX and Ecophage. The other authors declare that they have no competing interests. **Data, code, and materials availability:** Coordinates and structure factors of the LockinA–3′cADPR complex have been deposited in the Protein Data Bank under the accession number 9P8L. Data and materials are available in the main text or the supplementary materials. Other materials are available upon request. This research was funded in whole or in part by the Bill & Melinda Gates Foundation (INV-083469), a cOAlition S organization, and by the European Research Council (ERC-AdG GA 101018520); as required, the author will make the Author Accepted Manuscript (AAM) version available under a CC BY public copyright license.

SUPPLEMENTARY MATERIALS

science.org/doi/10.1126/science.aea1761
Figs. S1 to S4; Tables S1 to S7; MDAR Reproducibility Checklist

Submitted 30 June 2025; accepted 16 December 2025

10.1126/science.aea1761

Structural modeling reveals phage proteins that manipulate bacterial immune signaling

Nitzan Tal, Romi Hadary, Renee B. Chang, Ilya Osterman, Roy Jacobson, Erez Yirmiya, Nathalie Bechon, Dina Hochhauser, Miguel López Rivera, Barak Madhala, Jeremy Garb, Moshe Goldsmith, Tanita Wein, Philip J. Kranzusch, Gil Amitai, and Rotem Sorek

Science **391** (6789), eaea1761. DOI: 10.1126/science.aea1761

Editor's summary

When a bacterium is infected by a phage virus, it uses small signaling molecules to activate its defenses. Phages, in turn, have evolved ways to evade these defenses by capturing and "confiscating" the alert molecules, but how they do so has remained largely unknown. Tal *et al*. used artificial intelligence–based approaches to scan vast collections of phage proteins and identify factors that sequester or degrade immune signaling molecules (see the Perspective by Fedorova and Bondy-Denomy). The proteins they uncovered are found in thousands of phages, including the classic model phage T4 that has been studied for decades, and explain how phages overcome bacterial immune systems. Looking ahead, the approach described here could be applied to discover analogous proteins in viruses that infect animals and plants. —Di Jiang